

# Development of a two-dimensional coupled smoothed particle hydrodynamics model and its application to nonlinear wave simulations

Guixun Zhu, Jason Hughes, Siming Zheng <sup>\*</sup>, Deborah Greaves

*School of Engineering, Computing and Mathematics, University of Plymouth, Drake Circus, Plymouth PL4 8AA, UK*

## ARTICLE INFO

### Keywords:

Smoothed Particle Hydrodynamics  
Coupled model  
Open boundary  
Wave simulation  
Oscillating water column

## ABSTRACT

This paper presents a two dimensional two-way coupled model combining Smoothed Particle Hydrodynamics (SPH) based on the Navier–Stokes equations (NSE) and OceanWave3D based on the fully nonlinear potential flow theory (FNPT) in order to efficiently simulate non-linear waves and wave–structure interaction problems. The two models are strongly coupled in space and time domains using a fixed overlapping zone, wherein the information from both solvers is exchanged by relaxation functions. In the SPH model, an open relaxation boundary, which is implemented as open and relaxation zones, is used in the coupling region. Horizontal velocity and free surface elevation in the open and relaxation zones are obtained from OceanWave3D, while vertical velocity and density in the open zones are interpolated from the relaxation region. OceanWave3D requires the free surface elevation and vertical velocity at the free surface from SPH in the coupled region. The coupled model is tested by modelling a regular wave, irregular wave and wave over a submerged bar and an oscillating water column (OWC) device. The results demonstrate that the coupled model can produce satisfactory results with less computational time than the SPH-only model.

## 1. Introduction

Smoothed Particle Hydrodynamics (SPH) is a Lagrangian particle approach developed by Gingold and Monaghan [1], and Lucy [2] over forty years ago to explore difficulties in astrophysical dynamics. For its capacity to handle huge deformation issues, SPH is considered to be the ideal approach for modelling complicated interfacial flows [3–6]. The use of SPH-based models in coastal and offshore engineering has increased significantly over the years [7–10], owing to their excellent accuracy in studying wave transformation [11,12], wave breaking [13–15], and wave–structure interaction [16–20] processes. However, one of the SPH method's limitations is its poor computing efficiency, for which the most common solutions at the moment are hardware acceleration [21–26], particle refining methods [27–30], coupling approaches and numerical model of acceleration [31–33]. The goal of this research is to enhance computing efficiency by developing a coupling SPH-based wave tank. More specifically, the computationally expensive of SPH simulates the region with complex interfaces, while other efficient numerical models simulate the remaining area. This approach preserves the advantages of the SPH model while improving computational efficiency. However, it needs to develop accurate coupled models to ensure the reliability of the results.

Many coupled SPH models have been presented in the previous decade to simulate various problems. Narayanaswamy et al. [34] developed a two-way coupled model to combine the SPH model with

FUNWAVE, which is a finite difference model based on fully nonlinear Boussinesq equations, developed by Kirby et al. [35]. The overlap interface working as a moving boundary for the SPH model was located at the position far away from breaking regions. Altomare et al. [36] used a one-way coupling strategy to combine Simulating WAve till SHore (SWASH) with DualSPHysics. The waves in DualSPHysics were created by a moving boundary whose displacement in time was reconstructed using the velocities from SWASH. The main weakness was its inability to adjust for wave reflection at the moving border, where a moving boundary hybridization technique was applied. To solve this issue, a relaxation zone approach coupling between SWASH and DualSPHysics was later developed by Altomare et al. [37]. Napoli et al. [38] presented an FVM–SPH approach for incompressible flows, in which the interface was solved using an iterative method. The numerical results showed that the proposed hybrid approach can predict viscous flows and wave processes correctly with a significant reduction in computational efforts with respect to the standard SPH method. Marrone et al. [39] proposed a unique coupled SPH–FV technique with a transition zone. The coupled model was shown to be both accurate and practical in terms of CPU time and memory needs. The approach was later improved by Chiron et al. [40] to handle the net mass transfer and free surface transit over the coupling region. Zhang et al. [41] presented a 3D hybrid

\* Corresponding author.

E-mail address: [siming.zheng@plymouth.ac.uk](mailto:siming.zheng@plymouth.ac.uk) (S. Zheng).

model based on the SPH and the Quasi Arbitrary Lagrangian–Eulerian Finite Element Method (QALE-FEM) to study nonlinear wave–structure interaction. Verbrugghe et al. [42] presented a two-way coupled model between the DualSPHysics solver and the fully nonlinear potential flow solver OceanWave3D. An open boundary condition [42] was used at the coupling contacts inside the SPH numerical domain. The buffer particles were imposed at the entrance with horizontal orbital velocities and surface elevations determined using OceanWave3D. The SPH surface elevation was sent back into OceanWave3D, which overwrites the previously computed free surface. To hybridize shallow water equations-based SPH model with a Navier Stokes equations-based SPH model, Ni et al. [43] proposed a coupling scheme based on a non-reflective open boundary condition [44]. In addition, there are many other coupled models associated with the SPH method [45–50].

Note that different numerical models may not coincide with one another in terms of the underlying mathematical models (e.g., potential flow theory vs. NSE model). A coupled model combining different underlying mathematical models is mathematically inaccurate. For wave simulation applications in the far-field region, the use of formally simple control equations (as opposed to the Navier–Stokes equations) can lead to a simplification in the solution of the equations. This simplification is based on the simplification of fluid assumptions (e.g. potential flow theory assumes that the fluid is inviscid and irrotational). This can lead to an increase in computational efficiency. At the same time, it is reported that this coupling does not lead to a significant decrease in the accuracy of wave simulations. In addition, coupling on different discrete methods is common, e.g. mesh-mesh coupled models, and mesh-particle coupled models. This requires precise interpolation methods between the nodes of the different discrete methods. The couplings can be mainly classified into two categories: ‘one-way’ and ‘two-way’. One-way coupling, also known as ‘weak’ coupling, allows information to pass through the model in one direction. Whereas ‘two-way’ coupling (‘strong’ coupling) is more sensible as it allows information from both models to interact with each other. For spatially coupled regions, overlapping/non-overlapping approaches are both feasible. Non-overlapping coupling requires a matching of the physical quantities at the coupling interface. Overlapping coupling usually uses relaxation functions in the coupling region to achieve a transition of physical information. In addition, the coupling of different models may also involve the implementation of computer code.

In this work, a novel coupled model is developed in order to improve the computational efficiency of the SPH-based model without compromising the ability in dealing with non-linear problems for wave simulation. To the best of our knowledge, many of the existing coupled models do not consider free-surface coupling. Yet for wave simulation, it is necessary to ensure the coupling of the free surface at the coupling interface. Some others are one-way coupled models, meaning that for some circumstances the reflected waves generated in the SPH region cannot be transmitted through the coupling interface. In addition, the coupling interface may act as an inlet/outlet at the same time because of the wave motion. Nevertheless, in some existing models, the inlet and outlet boundaries are often treated differently.

In particular, this paper presents a two-dimensional two-way coupled model to hybridize the SPH model with OceanWave3D. OceanWave3D, based on fully nonlinear potential flow theory, is a very efficient and accurate simulation of surface waves and velocity fields from the deep sea, with satisfactory results both in the open ocean and nearshore. In the non-linear region (breaking wave and wave–structure interaction), the expensive SPH model is used to simulate the non-linear phenomena. While the remainder of the domain is simulated with OceanWave3D. The model is in a two-way coupling, i.e. the SPH model not only receives information from OceanWave3D but also feeds the information back to the OceanWave3D solver. Although the coupled SPH-OceanWave3D model [42] has been developed previously, the coupled model developed here uses different coupling techniques, mainly in terms of:

1. Different particle generation/deletion methods on the coupling interface. In [42], particle generation/deletion at the coupling interface is based on the position of the particle. While particle generation/deletion methods on the coupling interface in [40,51] have been used here (as Section 4.2.1).
2. The relaxation regions and relaxation function are used in the present coupled model. The relaxation region may result in the SPH region of the present model being larger than Verbrugghe et al. [42]’ model (as Section 4.2.2).
3. Free surface particle generation/deletion are used in the SPH model to achieve the coupling free surface level in the relaxation regions (as Section 4.2.2).
4. Moving least square reconstruction is used to obtain the pressure and vertical velocity of open regions (as Section 4.2.3).
5. The coupled model is implemented in an MPI-type parallel framework (as Section 4.4).

The remainder of this paper is organized as follows. The SPH model, OceanWave3D and the coupling strategy in this study are described in Sections 2, 3, and 4, respectively. Validations of the present model, including wave simulation, wave over a submerged bar, and simulation of onshore OWC devices, are described in Section 5. Finally, conclusions are drawn in Section 6.

## 2. SPH model

In this study, the flow in the SPH domain is assumed to be viscous, weakly-compressible, and adiabatic. The adopted governing equations consist of the Navier–Stokes equations in the Lagrange framework:

$$\begin{cases} \frac{du}{dt} = -\frac{1}{\rho} \nabla p + F_\alpha + g, \\ \frac{dp}{dt} = -\rho \nabla \cdot u, \\ \frac{dr}{dt} = u, \end{cases} \quad (1)$$

where  $\rho$ ,  $u$ ,  $t$ ,  $r$  and  $P$  denote the instant density, initial density, velocity vector, time, position vector and pressure, respectively.  $F_\alpha$  is the viscosity term and  $g$  represents the gravitational acceleration. The governing equation can be discretized by an  $\delta$ -SPH approximation. The  $\delta$ -SPH [29,52,53] formulation can be written as:

$$\begin{cases} \frac{d\rho_i}{dt} = -\rho_i \sum_j (\mathbf{u}_j - \mathbf{u}_i) \cdot \nabla_i W_{ij} V_j + \delta h c \sum_j \Psi_{ij} \cdot \nabla_i W_{ij} V_j, \\ \frac{du_i}{dt} = -\frac{1}{\rho_i} \sum_j (p_j + p_i) \cdot \nabla_i W_{ij} V_j + \alpha h c \sum_j \Pi_{ij} \nabla_i W_{ij} V_j + g, \end{cases} \quad (2)$$

where  $W$  is the kernel function (The renormalized Gaussian kernel [54] is used in this work.),  $c$  is numerical sound speed,  $h$  is the smoothing length,  $V$  is the volume of particles. If not specifically stated,  $\delta$  and  $\alpha$  are 0.1 and 0.01, respectively.

A density diffusion  $\Psi_{ij}$  is added to the continuity equation to avoid spurious numerical oscillations, and it can be written as

$$\begin{cases} \Psi_{ij} = 2(\rho_j - \rho_i) \frac{\mathbf{r}_j - \mathbf{r}_i}{|\mathbf{r}_j - \mathbf{r}_i|^2} - (\langle \nabla \rho \rangle_i^L + \langle \nabla \rho \rangle_j^L), \\ \langle \nabla \rho \rangle_i^L = \sum_j (\rho_j - \rho_i) L_i \nabla_i W_{ij} V_j, \quad \text{where } L_i = [\sum_j (\mathbf{r}_j - \mathbf{r}_i) \otimes \nabla_i W_{ij} V_j]^{-1} \end{cases} \quad (3)$$

where  $\otimes$  denotes tensor product. The  $\Pi_{ij}$  in the viscosity term is given as

$$\Pi_{ij} = \frac{(\mathbf{u}_j - \mathbf{u}_i) \cdot (\mathbf{r}_j - \mathbf{r}_i)}{|\mathbf{r}_j - \mathbf{r}_i|^2}. \quad (4)$$

Meanwhile, the fluid pressure is related to the density explicitly according to the concept of artificial compressibility. Then, the pressure is obtained through the equation of state as

$$P = (\rho - \rho_0)c^2, \quad (5)$$

where  $\rho_0$  is the initial density. In the present simulation, a prediction-correction time-stepping scheme is applied to ensure second-order accuracy [55]. Following Marrone et al. [53] and Bouscasse et al. [56], the present model uses the regular fixed ghost particles that are created to represent the solid boundary only.

### 3. OceanWave3D

OceanWave3D was proposed by Engsig-Karup et al. [57] and Bingham and Zhang [58] for large-scale modelling of wave problems in coastal and offshore environments, based on a fully non-linear potential flow theory. OceanWave3D numerically solves the potential flow governing equations [59] for gravity waves at the water surface in a 3D Eulerian reference system using a right-angle coordinate system  $(x, y, z)$ . Fluids are assumed to be incompressible, inviscid and non-rotating flows. The problem of non-breaking free surface waves can be described in terms of the velocity potential energy  $\phi$  and the  $z$  position  $\eta$  of the free surface. At a free surface, nodes should remain at the surface with a pressure equal to the atmospheric pressure. At the bottom, the no penetration condition is set. The kinematic and dynamic boundary conditions of the free surface, and bottom boundary condition are

$$\frac{\partial \eta}{\partial t} = -\frac{\partial \eta}{\partial x} \frac{\partial \phi}{\partial x} - \frac{\partial \eta}{\partial y} \frac{\partial \phi}{\partial y} + \tilde{w} \left[ 1 + \left( \frac{\partial \eta}{\partial x} \right)^2 + \left( \frac{\partial \eta}{\partial y} \right)^2 \right], \quad (6)$$

$$\frac{\partial \tilde{\phi}}{\partial t} = -\frac{1}{2} \left[ \left( \frac{\partial \tilde{\phi}}{\partial x} \right)^2 + \left( \frac{\partial \tilde{\phi}}{\partial y} \right)^2 \right] + \frac{1}{2} \tilde{w}^2 \left[ 1 + \left( \frac{\partial \eta}{\partial x} \right)^2 + \left( \frac{\partial \eta}{\partial y} \right)^2 \right] - g\eta, \quad (7)$$

$$\frac{\partial \phi}{\partial z} + \frac{\partial h_o}{\partial x} \frac{\partial \phi}{\partial x} + \frac{\partial h_o}{\partial y} \frac{\partial \phi}{\partial y} = 0, \quad z = -h_o, \quad (8)$$

where  $h_o = h_o(\mathbf{x})$  is the water depth from the seabed to the still water level.  $\tilde{\phi} = \phi(\mathbf{x}, \eta, t)$  is the velocity potential of the free surface,  $\mathbf{x} = (x, y)$  represents the horizontal position and  $\tilde{w}$  is the vertical velocity of the free surface.

The  $\sigma$  coordinate transformation allows a fixed grid distribution to be obtained taking into account free surface variations

$$\sigma = \frac{z + h_o(\mathbf{x})}{\eta(\mathbf{x}, t) + h_o(\mathbf{x})}. \quad (9)$$

Then Eqs. (6), (7) and (8) are rewritten as:

$$\Phi = \tilde{\phi}, \quad \sigma = 1; \quad (10)$$

$$\begin{aligned} \frac{\partial^2 \Phi}{\partial x^2} + \frac{\partial^2 \Phi}{\partial y^2} + \left( \frac{\partial^2 \sigma}{\partial x^2} + \frac{\partial^2 \sigma}{\partial y^2} \right) \frac{\partial \Phi}{\partial \sigma} + 2 \left[ \frac{\partial \sigma}{\partial x} \frac{\partial}{\partial x} \left( \frac{\partial \Phi}{\partial \sigma} \right) + \frac{\partial \sigma}{\partial y} \frac{\partial}{\partial y} \left( \frac{\partial \Phi}{\partial \sigma} \right) \right] + \\ \left( \frac{\partial^2 \sigma}{\partial x^2} + \frac{\partial^2 \sigma}{\partial y^2} + \frac{\partial^2 \sigma}{\partial z^2} \right) \frac{\partial^2 \Phi}{\partial \sigma^2} = 0, \quad 0 < \sigma < 1; \end{aligned} \quad (11)$$

$$\left( \frac{\partial \sigma}{\partial z} + \frac{\partial h_o}{\partial x} \frac{\partial \sigma}{\partial x} + \frac{\partial h_o}{\partial y} \frac{\partial \sigma}{\partial y} \right) \frac{\partial \Phi}{\partial \sigma} + \frac{\partial h_o}{\partial x} \frac{\partial \Phi}{\partial x} + \frac{\partial h_o}{\partial y} \frac{\partial \Phi}{\partial y} = 0, \quad \sigma = 0. \quad (12)$$

The classical fourth-order Runge–Kutta method is used as the numerical integration algorithm. Wave generation and absorption are achieved using the relaxation zone method proposed by Larsen and Dancy [60].

### 4. Coupling strategy

The coupled model is based on the decomposition of a global domain into separated OceanWave3D and SPH domains. The exchange of information between OceanWave3D and SPH domains is performed by a two-way coupling algorithm, and the couplings take place by using relaxation functions to the physical properties in the coupling region. This is presented in four main sections: coupling strategies in space and time, Open relaxation region in the SPH model, OceanWave3D solver for the coupled model, and coupling strategies for the parallel system.

#### 4.1. Coupling strategies in space and time

In the current coupled model the whole computational domain is spatially divided into several overlapping sub-domains. Fig. 1 shows an example of the coupled model. The computational domain is divided into OceanWave3D and SPH regions. The coupling regions are fixed and carry out information transfer. The OceanWave3D and SPH models have different requirements for time steps. For accurate and stable calculations, models need to be coupled at the same moments in time. The time step ( $t_o$ ) for OceanWave3D is typically several orders of magnitude higher than ( $t_s$ ) for SPH. In general, the simulation of the OceanWave3D domain is less computationally expensive than the SPH domain. Therefore, the unique time step is used

$$t_o = t_s. \quad (13)$$

The coupling strategy here is to complete the calculation at each time step and then couple the results of the two models, as shown in Fig. 2. At the beginning of a time step, the results of OceanWave in the coupled region are passed into the SPH model. After SPH has completed its calculations for a time step, its data is passed back into OceanWave3D. OceanWave3D then completes the calculation for one time step.

Note that SPH and Oceanwave3D take the same time step in the coupled model. SPH and OceanWave3D are coupled in time and space, and so at each time step, the SPH needs information from OceanWave3D. Using the same time step is the simplest and most direct way of coupling. The computing speed of the OceanWave3D solver is much faster than that of the SPH solver (See Tables 2 and 3), therefore, even if the same time step is adopted, the amount of computation will not increase much.

#### 4.2. Open relaxation boundary in SPH model

The length of a numerical flume is often tens or even hundreds of metres. The SPH computational domain can be truncated and coupled with OceanWave3D. The development of the coupled model shortens the size of the SPH computational domain. It is necessary to develop open boundaries at the SPH coupling interface. The open boundary can be transformed between the incoming and outgoing flow boundaries because of the periodicity of wave flow. In many articles, the authors treat inlet and outlet boundaries separately [61,62], but it needs to develop stable inlet/outlet flow open boundaries. According to the wave motion properties, the velocity is not uniform over a cross-section that propagates along the wave. This means that the open flow field particle generation/deletion is not uniformly distributed perpendicular to the open boundary, and appears at the open boundary. Irregular particle distributions may lead to calculation errors. As the free surface level is always constantly changing in the coupling area, the increase and decrease of particles in the vertical direction should be considered.

In order to achieve the above, an open relaxation boundary is developed. The open relaxation boundaries are implemented as open and relaxation zones. Particles in these zones are called open particles and relaxation particles, respectively. Physical quantities from OceanWave3D can be applied to these particles. A sketch of the open relaxation boundary is depicted in Fig. 1. The relaxation zone, where a relaxation function is used, can obtain a smooth transitional region from the results of OceanWave3D to SPH simulations. The open zones are placed in the inflow/outflow regions to cover the truncated kernel area. The number of open particle layers is determined by the kernel function and the size of compact support. Therefore, the SPH model achieves coupling in the coupled region by the open relaxation boundary. Meanwhile, the open relaxation boundary ensures that the SPH model does not collapse due to kernel truncation in the coupling region. In the following, the treatments of open particles and relaxation particles are discussed in detail.

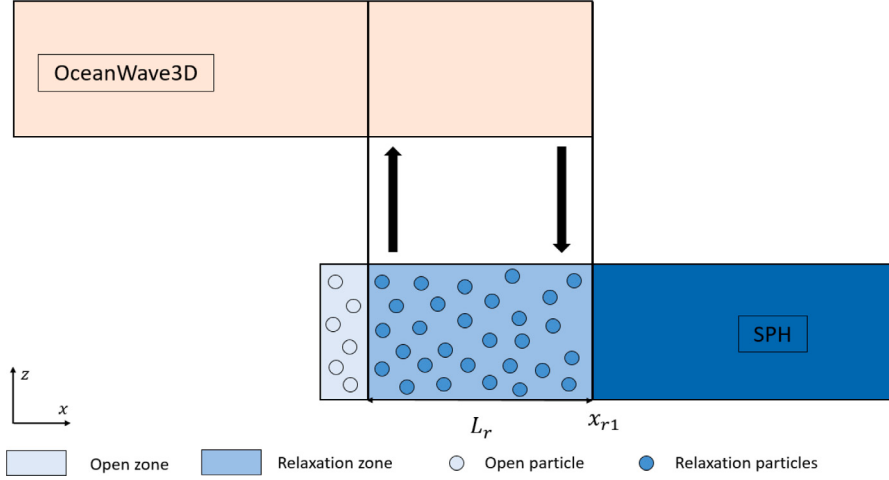


Fig. 1. Sketch of coupling sub-domain.

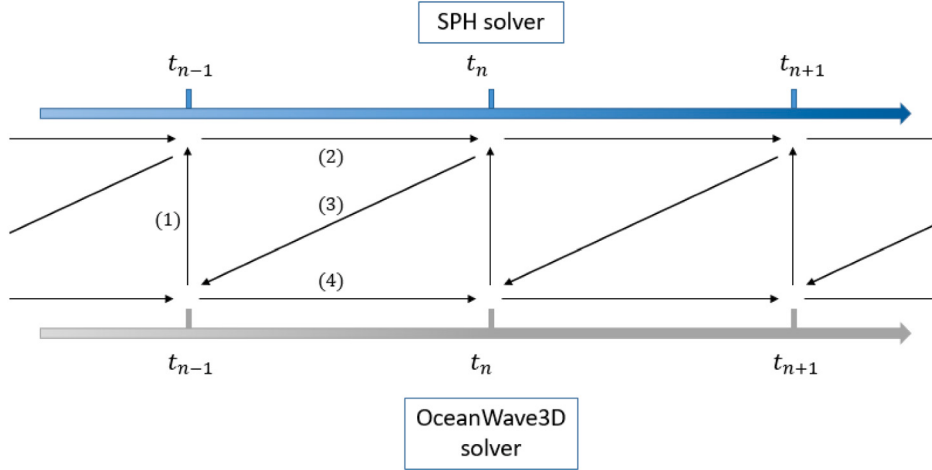


Fig. 2. Sketch of calculation process under one time step.

#### 4.2.1. Particle creation/deletion/transformation

At the open relaxation boundary, particles transform between open and relaxation particles. At the same time, the mass flux at the coupling interface is achieved by the production and deletion of the open particles. The position is used as a basis to distinguish particle species. An open particle entering the relaxation region is transformed into a relaxation particle. Relaxation particles and fluid particles are updated based on the change of position. Meanwhile, the positions of each kind of particle are updated according to the velocity in the time integration method.

Particle generation and deletion at coupling interfaces can lead to sharp changes in mass at the interface. To solve that, the interface is subdivided into segments of equal size [51]. Mass flux at each segment is obtained from OceanWave3D. Meanwhile, the change in mass due to the creation and deletion of particles is applied to the interface segment to ensure a continuous change in mass at the interface over time. The mass flux  $m_f$  across each segment from OceanWave3D is given by:

$$m_f = \rho_s \Delta x_s \mathbf{u}_{sg} \mathbf{n}_s \Delta t, \quad (14)$$

where  $\mathbf{u}_{sg}$  and  $\rho_s$  are the velocity and density at the center of the segment from the underlying OceanWave3D field, respectively. The symbols  $\mathbf{n}_s$  and  $\Delta x_s$  represent the normal vector pointing to the interior of the SPH and the width/area of each segment, respectively. The symbols for mass fluxes indicate mass inflow and outflow into the SPH region. The mass of each segment at each time step is calculated

as [40,51]

$$m_s^{n+1} = m_s^n + m_f^n + m_{a/d}^n, \quad (15)$$

where  $n+1$  and  $n$  denote  $n+1$  time step and  $n$  time step, respectively.  $m_f^n$  and  $m_{a/d}^n$  denote mass flux and the change of mass due to particle generation  $m_g^n$  and deletion  $m_d^n$  at  $n$  time step. Fig. 3 shows the process of particle generation and deletion. When the segmented mass  $m_s$  exceeds the mass of a reference particle, a new particle is injected and the value of the resulting mass is subtracted from the corresponding segmented mass. Conversely, when this mass is lower than the mass of the reference particle, the particle closest to the segment is removed and its mass is added to the mass of the segment. Furthermore, particles that move outside the open boundary are removed and, again, their mass is added to the nearest segment. A weight  $w_s$  [51] is associated to these mass change in Fig. 3, can be calculated as

$$w_{s1} = \frac{r_1}{r_s}, \quad (16)$$

$$w_{s2} = \frac{r_2}{r_s} = 1 - w_{s1}, \quad (17)$$

where  $r_s$ ,  $r_1$ , and  $r_2$  are the length of the segment, the vertical distance between the particle and the centre of segment 1, and the vertical distance between the particle and the centre of segment 2. The change of mass due to particle deletion  $m_d^n$  in Fig. 3 for segment 1 and 2 can

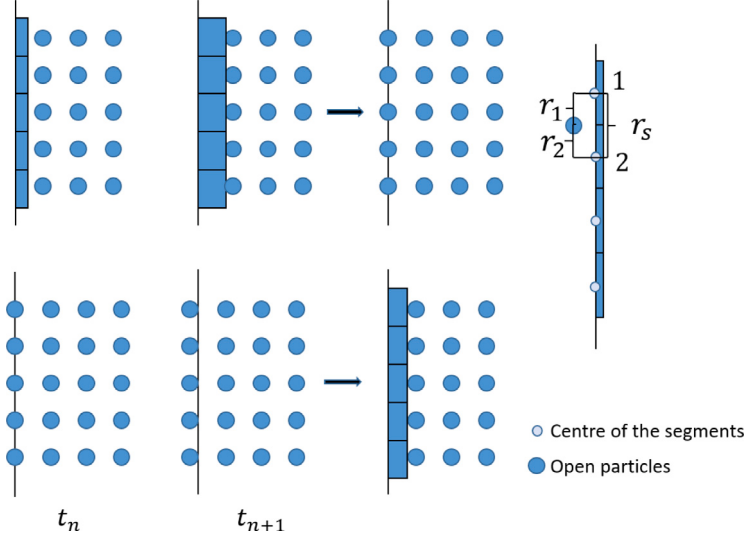


Fig. 3. Sketch of particle generation and deletion at coupling interface.

be calculated as

$$m_{d1}^n = m_p w_{s1}, \quad (18)$$

$$m_{d2}^n = m_p w_{s2}, \quad (19)$$

where  $m_{d1}^n$  and  $m_{d2}^n$  are the mass change of segments 1 and 2 due to particle deletion.  $m_p$  denotes the mass of particles. The presence of weights ensures that the changes in mass are distributed over adjacent segments.

#### 4.2.2. Relaxation particles

Relaxation zones are implemented to establish the smooth continuum of horizontal velocity and free surface level in the relaxation region from the Oceanwave3D to the SPH results. Horizontal velocity and free surface level from OceanWave3D are imposed on these relaxation particles. The relaxation domain builds smooth transitions. A relaxation function is applied here, which is an extension to that of Mayer et al. [63] and has been used in [64]. The relaxation function is

$$\alpha_r(i) = 1.0 - \frac{\exp(\chi_{rs}^\beta) - 1}{\exp(1) - 1}, \quad i \in R1, \quad (20)$$

where  $\beta = 3.5$  is relaxation coefficient and  $\chi_{rs} = \frac{|x_i - x_{r1}|}{L_r}$ .  $x_{r1}$  are the horizontal positions of the interfaces between the relaxation particle zone and the fluid zone, as shown in Fig. 1.  $R1$  denotes the coupling region.  $x_i$  is the horizontal position of particle  $i$ .  $L_r$  denotes the length of the relaxation zone. The length of the relaxation region refers to the size of the relaxation region along the direction of wave propagation in SPH solver (as Fig. 1). The length of the relaxation region is the same as the length of the coupling region. The definition of  $\chi_{rs}$  ensures that  $\alpha_r$  is always 1 at the interfaces between the fluid zone and the relaxation zones, and  $\alpha_r$  is always 0 at the interfaces between the open zones and the relaxation zones. Then the horizontal velocity  $u_x$  and free surface level  $\eta$  is modified in the following way

$$\Phi_a = \alpha_r(\Phi_a)^{SPH} + (1 - \alpha_r)(\Phi_a)^{OceanWave3D}. \quad (21)$$

where  $\Phi_a$  denote horizontal velocity and free surface level. Once the corrected free surface level  $\eta_i$  is obtained,  $\eta_i$  is imposed on relaxation particles. In the relaxation zone, the fluid particles near the free surface are generated or removed in reference to the corrected free surface level  $\eta_i$  as shown in Fig. 4. To achieve that, all free surface particles need to be detected inside the relaxation zone using the method proposed by Marrone et al. [65]. The height of each free surface particle is

compared with the corrected free surface level  $\eta_i$  at the corresponding position. A free surface particle is removed if it goes up above  $\eta_i$  with a longer distance than the initial particle spacing. If the free surface particle goes down below  $\eta_i$  with a longer distance than the initial particle spacing, a new open particle is generated. The physical information of the new particles refers to the information of the height of the free surface particles. The new fluid particle has the same horizontal coordinates as the previous free surface particle, but the vertical height is one initial particle spacing greater than the previous free surface particle. The velocity of the new particle is set to the same as that of the original free surface particle.

Due to the use of relaxation functions in the relaxation zone, a smooth result is constructed between the SPH results and the OceanWave3D results. The different results produced by the two numerical models will gradually be harmonized. As the reflected wave passes into the relaxation region, the motion of the particles gradually converges to the OceanWave3D solution due to the relaxation function.

#### 4.2.3. Open particles

The main purpose of open particles is to avoid the effects of kernel truncation. Due to the use of the relaxation zone, the horizontal velocity of the flow field, at the interface between the relaxation zone and the open zone, achieves the same solution as OceanWave3D. To obtain the vertical velocity and density of the open particles, interpolation nodes are used. Along the normal direction of the open boundary, the interpolation nodes are arranged at the open boundary line as shown in Fig. 5. In the vicinity of the interpolation node, SPH interpolation does not give good results due to the presence of kernel truncation. Thus, a moving least-squares (MLS) reconstruction is used to get the physical properties of open particles.

Suppose that  $f(\mathbf{r})$  is the local pressure or velocity field function in the support domain of interpolation nodes. The approximation of  $f(\mathbf{r})$  at the position of relaxation particles is denoted as  $f_h(\mathbf{r})$ , which can be calculated with the help of a basis as:

$$f_h(\mathbf{r}) = \sum_{i=1}^{mn} q(\mathbf{r}_i) c_m(\mathbf{r}_i) = q^T(\mathbf{r}) c_m(\mathbf{r}), \quad (22)$$

where  $q(\mathbf{r})$  is the basis function and  $mn$  is the term numbers of the basis function,  $c_m$  is the factor of the basis function. In this work, the quadratic basis is used as

$$q^T(\mathbf{r}) = [1, x, y, x^2, xy, y^2], mn = 6. \quad (23)$$

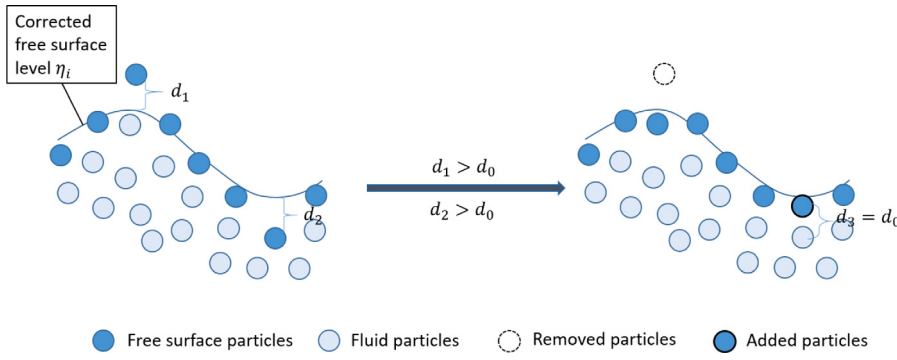


Fig. 4. Sketch of generation and removal of free surface particles in the relaxation zone.

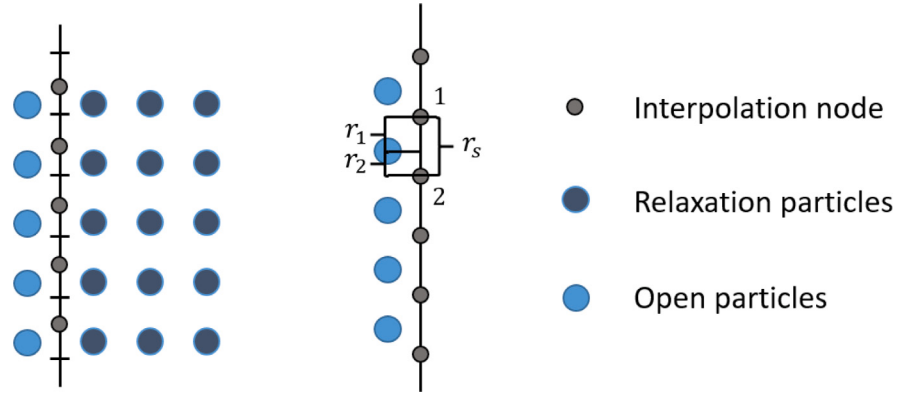


Fig. 5. Sketch of interpolation for open particles.

Since pressure and velocity are interpolated,  $f_h(\mathbf{r})$  can denote the local pressure and velocity reconstruction field here and is influenced by the nearby relaxation particles. Thus, it can construct a function of weighted residual  $Q$ :

$$Q = \sum_{j=1}^n W_q(\mathbf{r}_j)(f_h(\mathbf{r}_j) - f(\mathbf{r}_j))^2 = \sum_{j=1}^n W_q(\mathbf{r}_j)[(q^T(\mathbf{r}_j)c_m(\mathbf{r}_j) - f(\mathbf{r}_j))^2], \quad (24)$$

where  $W_q(\mathbf{r})$  is a weight function,  $n$  is the number of the relaxation particles inside the support domain of the weight function. The renormalized Gaussian kernel [54] is used as the weight function in this work.

For an arbitrary relaxation particle, the value of  $c(\mathbf{r})$  can be determined by minimizing the weighted residual  $Q$

$$\frac{\partial Q}{\partial c} = \mathbf{G}(\mathbf{r})c_m(\mathbf{r}) - \mathbf{H}(\mathbf{r})\mathbf{F}_q = 0, \quad (25)$$

where  $\mathbf{G}(\mathbf{r})$  is given as

$$\mathbf{G}(\mathbf{r}) = \sum_{j=1}^n W_q(\mathbf{r}_j)q^T(\mathbf{r}_j)q(\mathbf{r}_j), \quad (26)$$

and  $\mathbf{H}(\mathbf{r})$  is given as

$$\mathbf{H}(\mathbf{r}) = q^T(\mathbf{r})W_q(\mathbf{r}) = [q(\mathbf{r}_1)W_q(\mathbf{r}_1), q(\mathbf{r}_2)W_q(\mathbf{r}_2), \dots, q(\mathbf{r}_n)W_q(\mathbf{r}_n)], \quad (27)$$

and  $\mathbf{F}_q$  is field value

$$\mathbf{F}_q = [f_1, f_2, \dots, f_n], \quad (28)$$

Solving for  $c_m(\mathbf{r})$  from Eq. (25) and substituting it into Eq. (22) leads to

$$f_h(\mathbf{r}) = q^T(\mathbf{r})\mathbf{G}^{-1}(\mathbf{r})\mathbf{H}(\mathbf{r})\mathbf{F}_q = Y^T(\mathbf{r})\mathbf{F}_q, \quad (29)$$

where  $Y^T(\mathbf{r})$  is the shape function. The pressure and vertical velocity of interpolation nodes can be obtained from  $f_h(\mathbf{r})$ . Meanwhile, the pressure gradient of interpolation nodes can be calculated by the gradient

of  $f_h(\mathbf{r})$  as

$$f'_h(\mathbf{r}) = (Y^T(\mathbf{r}))'\mathbf{F} = ((q^T(\mathbf{r}))'\mathbf{G}^{-1}(\mathbf{r})\mathbf{H}(\mathbf{r}) + q^T(\mathbf{r})(\mathbf{G}^{-1}(\mathbf{r}))'\mathbf{H}(\mathbf{r}) + q^T(\mathbf{r})\mathbf{G}^{-1}(\mathbf{r})(\mathbf{H}(\mathbf{r}))')\mathbf{F}_q. \quad (30)$$

The pressure field at the open boundary enforces the Neumann boundary condition. Considering the right-hand sketch of Fig. 5, the pressure of an ordinary ghost particle is evaluated as follows

$$p_o = (p_{i1} + r_{i0}p_{i2}^n\rho_{i1})w_{i1} + (p_{i2} + r_{i0}p_{i1}^n\rho_{i2})w_{i2}, \quad (31)$$

where  $w_{i1}$  and  $w_{i2}$  are the weights of interpolation nodes. The weights in Fig. 5 are calculated in the same way as in Fig. 3.  $p_{i1}^n$  and  $p_{i2}^n$  denote the gradient of pressure at interpolation nodes 1 and 2, respectively.  $p_{i1}$  and  $p_{i2}$  denote the pressure at interpolation nodes 1 and 2, respectively. The vertical velocity of the ghost particle can be obtained using the same method. The position of the open particle is obtained with the horizontal velocity. The update of the vertical position of particles is not changed in the paper. The new open particle location from particle generation is set in the center of the segment (see Section 4.2.1).

#### 4.2.4. SPH results for OceanWave3D

In addition to coupling physical quantities from OceanWave3D, the SPH model also needs to interpolate physical quantities and pass them into OceanWave3D. In OceanWave3D, only free surface quantities can be coupled. Thus, the coupling is limited to the surface elevation and the vertical free surface velocity, yielding satisfactory results. The vertical free surface velocity  $\tilde{u}^u$  can be obtained by SPH interpolation

$$\tilde{u}_i^u = \frac{\sum_{j \in fluid} w_j^u W_{ij} V_j}{\sum_{j \in fluid} W_{ij}}, \quad (32)$$

where  $i$  is the node located at the free surface in OceanWave3D,  $j$  is the fluid particle in SPH, and  $w_j^u$  is the vertical velocity of particle  $j$ .

#### 4.3. OceanWave3D for coupled model

In the coupling region, the SPH solver needs velocity and free surface level data from OceanWave3D. In order to transfer the OceanWave3D results to SPH, the interpolation of the data in the coupling region should be calculated. Generally, the particle positions of SPH and the node positions of OceanWave3D do not coincide in the coupled region. Therefore, the reference physical properties of the particles need to be obtained by interpolation at the nodes. Following the approach in [66], the native pre-computed finite difference stencils of the solver are utilized for efficient evaluation of the following finite Taylor series:

$$\mathbf{N}_i(\mathbf{x}_i + \Delta\mathbf{x}_i) = \sum_{n=0}^{2a} \frac{\Delta^n}{n!} \frac{\partial^n \mathbf{N}_i}{\partial \mathbf{x}_i^n}, \quad (33)$$

where  $\mathbf{N}_i(\mathbf{x}_i + \Delta\mathbf{x}_i)$  is the reference value of the SPH particle  $i$  at the position  $\mathbf{x}_i + \Delta\mathbf{x}_i$ .  $\mathbf{x}_i$  is the position of the OceanWave3D node, which is the nearest neighbour node to SPH particle  $i$ . In the interpolation kernel,  $2a+1$  terms are applied ( $a = 2$ ). Generally speaking, there is some error between the free surface height of SPH and the OceanWave3D results. This means that SPH particles may exist outside the OceanWave3D grid nodes. If so, the grid in the vertical direction is directly selected as the highest node point.

As mentioned previously, the SPH particles in the open relaxation zone require velocity and free surface level from OceanWave3D. When the velocity potential  $\Phi$  is obtained in the  $\sigma$ -domain, the velocities can be calculated as follows:

$$u(x, z) = \frac{\partial \Phi(\mathbf{x}, z)}{\partial x} = \frac{\partial \Phi(\mathbf{x}, \sigma)}{\partial x} + \frac{\partial \sigma}{\partial x} \frac{\partial \Phi(\mathbf{x}, \sigma)}{\partial \sigma}, \quad (34)$$

$$v(\mathbf{x}, z) = \frac{\partial \Phi(\mathbf{x}, z)}{\partial y} = \frac{\partial \Phi(\mathbf{x}, \sigma)}{\partial y} + \frac{\partial \sigma}{\partial y} \frac{\partial \Phi(\mathbf{x}, \sigma)}{\partial \sigma}, \quad (35)$$

$$w(\mathbf{x}, z) = \frac{\partial \Phi(\mathbf{x}, z)}{\partial z} = \frac{\partial \sigma}{\partial z} \frac{\partial \Phi(\mathbf{x}, \sigma)}{\partial \sigma}. \quad (36)$$

In the present coupled model, the free surface level and vertical free surface velocity inside the open relaxation boundary are transferred, as shown in Fig. 1. To ensure a smooth transition from SPH results to OceanWave3D data, the same relaxation function as the one in the SPH model is used.

#### 4.4. Coupling strategies for parallel system

Both the SPH and OceanWave3D codes are written in Fortran. However, the current SPH code is MPI-parallel and the OceanWave3D code is not parallel. Therefore, when coupling the two models, the coupling strategies under a parallel system is achieved. Since OceanWave3D is much more computationally efficient than SPH, a processor is used to run the OceanWave3D results separately. In the parallel SPH model [67,68], it can determine which processors in the SPH model have information that needs to be passed to OceanWave3D, based on the location of those processors. The Verbrugghe et al. [42,48]' model used Python to pass and treat the information between the two models, leading to an implementation that can be extended further to other wave propagation models. Whereas the coupling process in the present work is implemented at the code level. Data transfer can be implemented directly through point-to-point MPI communication. The data is passed using *MPI – send* and *MPI – receive*.

A detailed flowchart of the developed framework is attached in Fig. 6. The code is written in FORTRAN using open-source libraries OpenMPI. If not specifically stated, studies in this paper are conducted on the Fotcluster2 in High Performance Computer Centre at the University of Plymouth. Fotcluster2 is a 752-core distributed-memory cluster, which is comprised of: a 3U combined head & storage node, plus 56 compute nodes. The tests are conducted on the phase2 consisting of 36 Viglen HX425T<sup>2</sup>i HPC 2U Compute Nodes, equipped with Dual Intel

Xeon E5650 (Westmere) Six Core 2.66 GHz processors and 12 GB of memory per motherboard.

### 5. Numerical validation

#### 5.1. Regular wave

The simulation of non-linear regular waves is to verify the accuracy of the coupling scheme. Another important part is to demonstrate the contribution of coupled models in reducing computational costs by comparing the simulation time of different models. The numerical domain for the coupled model is shown in Fig. 7, where a 40 m long wave tank is defined. On the right side of the tank, a 5 m-long sponge layer is applied to absorb waves. On the left side of the tank, part of the OceanWave3D region, a 4 m-long relaxation area is used to generate waves.  $L_a$  and  $L_b$  are the beginning and ending positions of the coupling region. A second-order Stokes wave with a wave height of 0.1 m and wave period of 2.0 s is used to validate the coupled model. The mean average errors for amplitude  $MAE_a$  and phase  $MAE_p$  [69] are calculated. Fig. 8 shows the free surface elevation for various regular wave cases at 25 m. Table 1 summarizes the numerical settings and errors of regular wave cases.

Comparing the results of cases (1), (2), (3), (4), and (5), it can be found that the variation in mesh size of OceanWave3D does not show much effect on the coupled simulation results. By comparing cases (1), (6), and (7), it is found that as the particle spacing decreases, it gradually approximates the analytical solution. When the particle spacing is less than 0.01 m, it does not show a higher agreement with the theoretical solution. In this case, the wave height is 0.1 m, the particle spacing is 0.01 m, and the ratio of wave height to particle spacing is ten. This result is consistent with the results of Roselli et al. [70] and Altomare et al. [12] on the selection of particle spacing and wave height.

The comparison between cases (1), (8), and (9) indicates that the results are more accurate as the length of the coupling region increases. The wave case simulated solely by OceanWave3D is better matched to the theoretical solution those when simulated by SPH or the coupled model according to cases (1), (10), and (11). SPH model is based on the NSE, which takes into account fluid viscosity and rotation. In the simulation of wave propagation, the results gradually deviate from the theoretical solution over time in these cases, due to the fluid viscosity as well as numerical dissipation [71]. Fig. 9 shows the pressure field of cases (1), (10), and (11) at 11 s. It is found that the coupled model, SPH-only, and OceanWave3D have a smooth pressure field. Fig. 10 shows the velocity field of cases (1). A smooth horizontal and vertical velocity field is found near the coupling interface.

Fig. 11 compares the free surface history at 25 m between the current coupled model and Verbrugghe et al. [42]' model. The numerical setting is the same as the model in this paper, except that the coupled model is different. The coupled model in this paper is more consistent than the results of the Verbrugghe et al. [42]' model at the local peak value of the free surface after  $t/T = 10.0$ . Fig. 12 compares the pressure, horizontal velocity, and vertical velocity fields near the coupling interface between the current coupled model and the Verbrugghe et al. [42]' model. The current coupled model is smoother and more stable in pressure and velocity distribution. The Verbrugghe et al. [42]' model corrects the horizontal velocity in the open boundary, resulting in discontinuous velocity and disturbances. In the present model, the relaxation function is applied to realize a smooth transition of the physical quantity. Therefore, the coupling interface shows smooth and stable results from the present coupled model.

Table 2 presents the time cost of the regular wave cases. Comparing the results of cases (1), (2), (3), (4), and (5), the number of meshes has little effect on the calculation cost because the cost of OceanWave3D is relatively small. By comparing cases (1), (6), and (7), it is found that the increasing SPH particle numbers (high particle resolution)

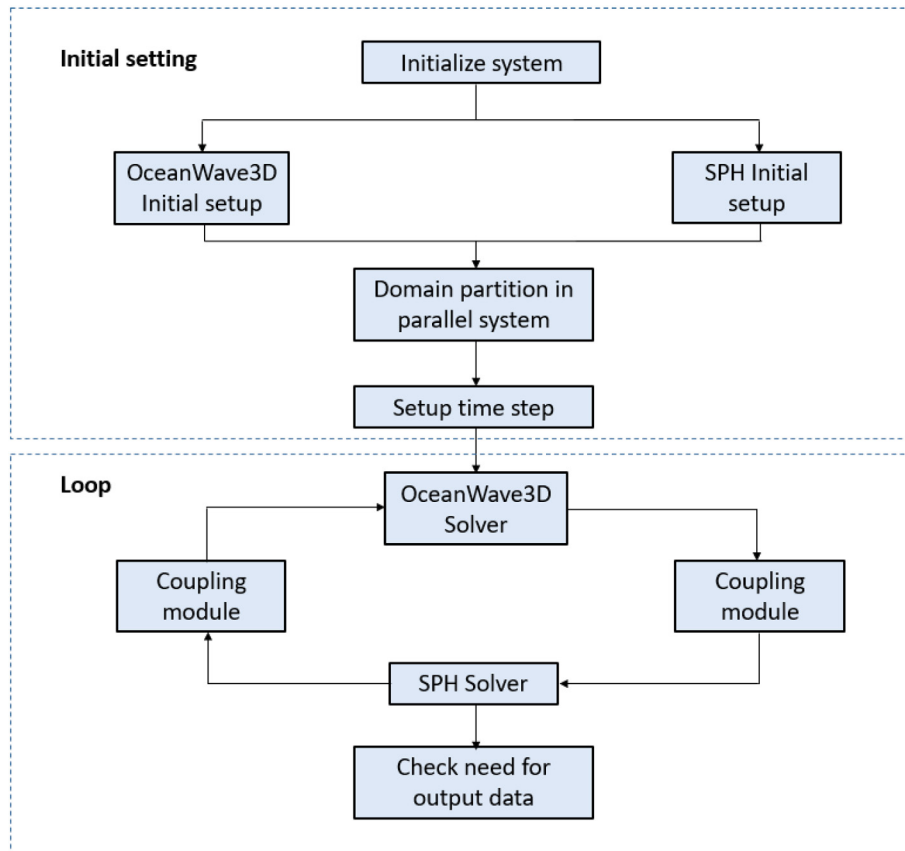


Fig. 6. Flowchart of coupled model framework.

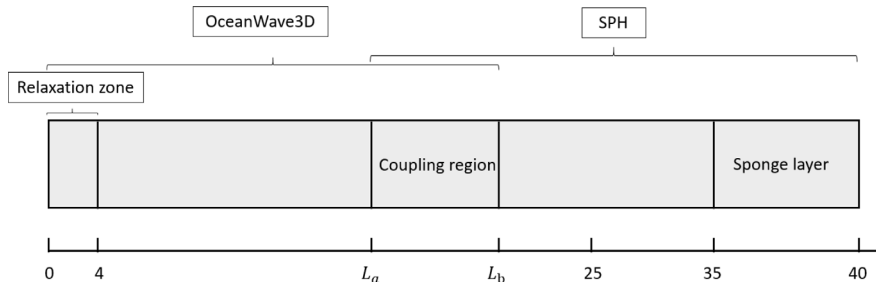


Fig. 7. Computation domain for wave simulation cases.

Table 1

Numerical setup, errors and cost of the regular wave cases.

Case	Mesh numbers ( $x, y$ )	Particle size (m)	Particle number	$L_a$ (m)	$L_b$ (m)	$MAE_a$	$MAE_p$	Cores
1	$900 \times 10$	0.01	175 000	15.0	19.6	3.2%	2.9%	49
2	$1800 \times 10$	0.01	175 000	15.0	19.6	3.2%	2.9%	49
3	$450 \times 10$	0.01	175 000	15.0	19.6	5.2%	3.0%	49
4	$900 \times 20$	0.01	175 000	15.0	19.6	3.2%	2.9%	49
5	$900 \times 5$	0.01	175 000	15.0	19.6	3.2%	2.9%	49
6	$900 \times 10$	0.02	43 750	15.0	19.6	5.0%	3.5%	49
7	$900 \times 10$	0.005	700 000	15.0	19.6	3.1%	2.9%	49
8	$900 \times 10$	0.01	175 000	15.0	17.3	3.4%	3.1%	49
9	$900 \times 10$	0.01	175 000	15.0	21.9	3.1%	2.9%	49
10	$2400 \times 10$	—	—	15.0	19.6	2.5%	2.3%	1
11	—	0.01	280 000	15.0	19.6	3.6%	2.9%	48

leads to an increase in the cost of coupling modules. However, the proportion of the cost of the coupling module decreases. As the particle number increases, the increase in SPH cost is greater than the increase in coupling module cost. The comparison between cases (1), (8), and (9) indicates that the total calculation cost and the cost of the coupling

module increase with the increase in relaxation domain length. The main reason is that the increase of the relaxation domain leads to an increase in the number of particles that need interpolation in the coupling module. The computational cost of the coupled model is less than the cost of the SPH-only model, but much more than the cost of

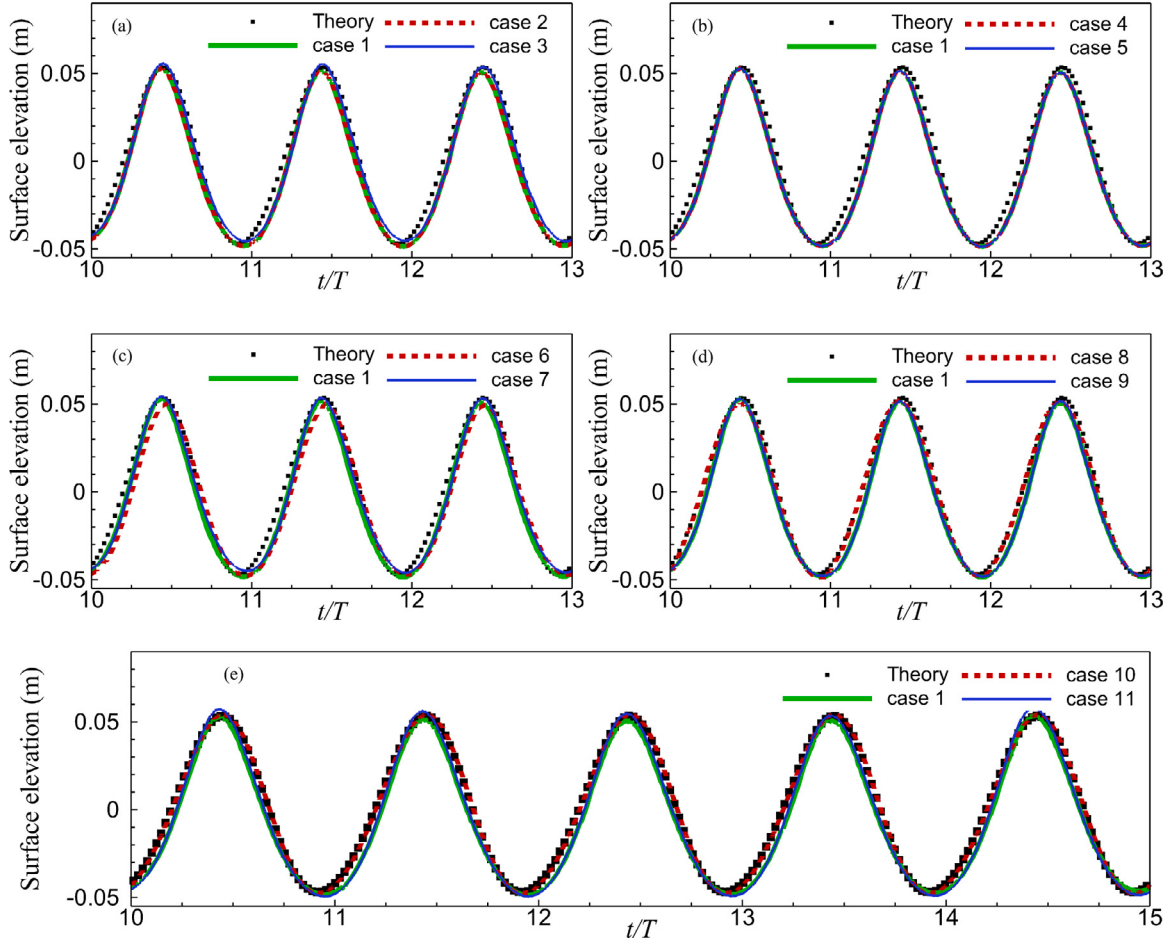


**Fig. 8.** Free surface at 25 m comparison between numerical simulation and theory solution for the regular waves.

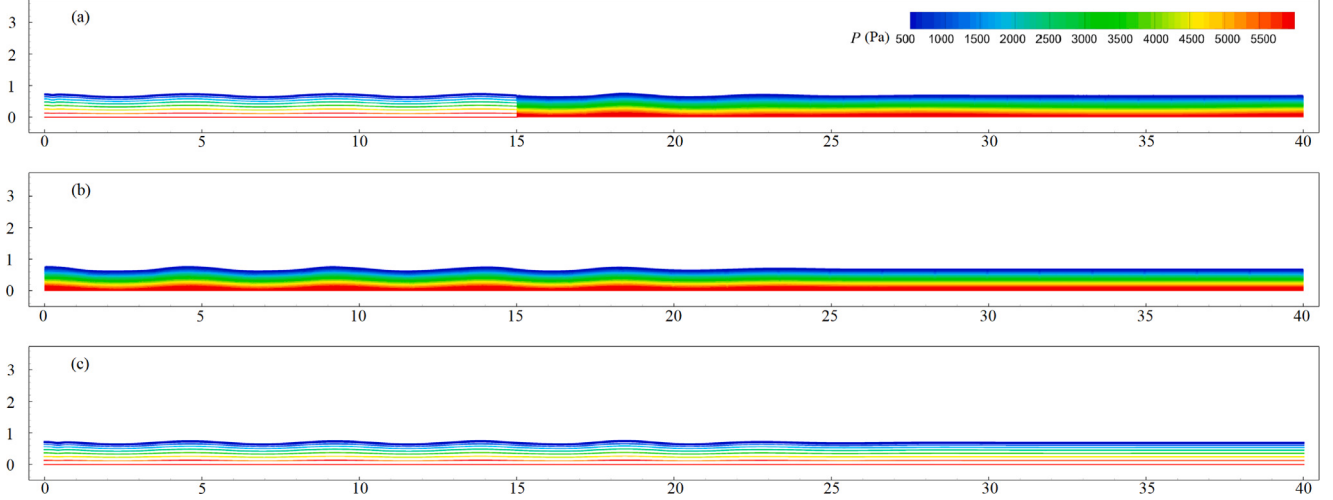


**Fig. 9.** Pressure field comparison between coupled model (a), SPH (b), and OceanWave3D (c) for regular waves.

OceanWave3D according to cases (1), (10), and (11). The cost of the coupling module is about 15% of the total cost of the coupled model. Therefore, the coupled model can reduce the cost of computation, and the cost of the coupling module is relatively small. The relaxation region in the SPH solver is not used by Verbrugge et al. [42], and the number of particles required by the coupling interpolation is small (only particles in the open region). In addition, the free surface particle

generation/interpolation technique is not considered in their model, and different interpolation methods are used. Therefore, the overall cost of the Verbrugge et al. [42]' model is less than the present model. Overall, the current model provides a smooth coupled interface and accurate results, but it is more expensive than the Verbrugge et al. [42]' model.

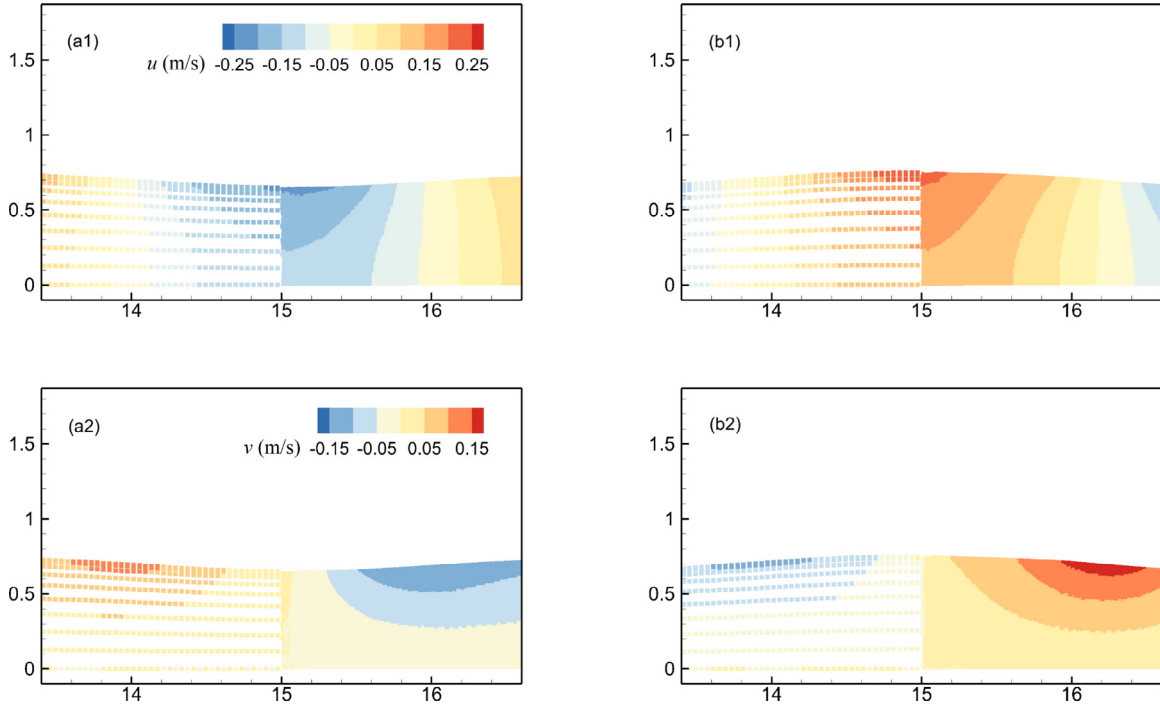


**Fig. 10.** Velocity field of regular waves near coupling region at  $t = 13.5$  s and  $14.5$  s. (Labels ‘a’ and ‘b’ denotes  $13.5$  s and  $14.5$  s, respectively; Label ‘1’ and ‘2’ denotes horizontal velocity and vertical velocity, respectively.).

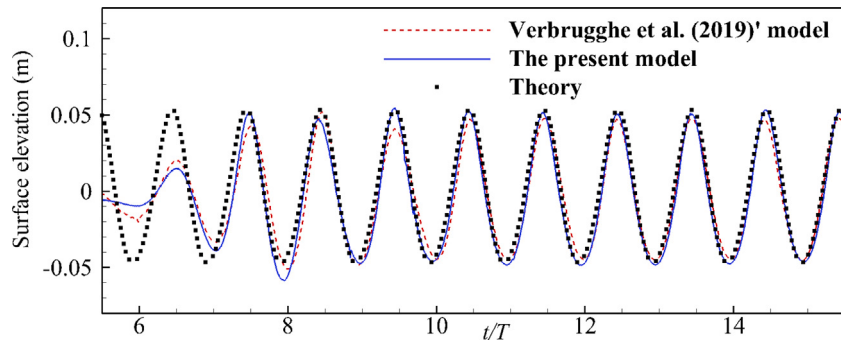


**Fig. 11.** Free surface at 25 m comparison between the present coupled model, Verbrugghe et al. [42]’ model and theory solution for the regular waves.

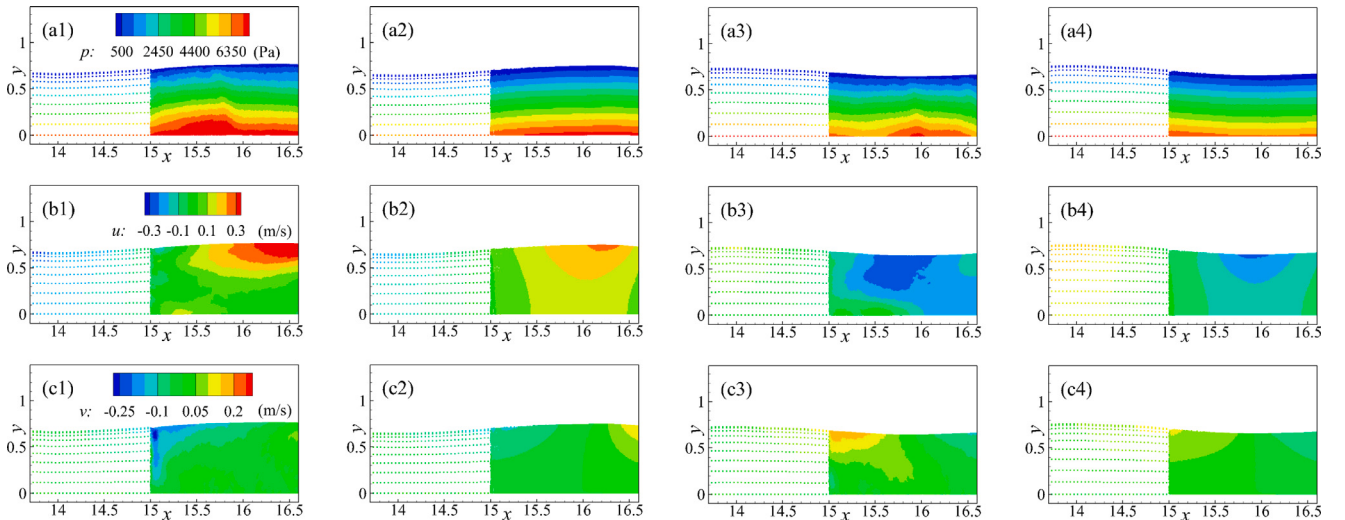


**Fig. 12.** Contour plot of the pressure (a), horizontal velocity (b), and the vertical velocity (c) of the regular wave case. (Labels ‘1’ and ‘2’ denote results of Verbrugghe et al. [42]’ model and the present coupled model at  $15.0$  s, respectively; Labels ‘3’ and ‘4’ denote results of Verbrugghe et al. [42]’ model and the present coupled model at  $20.0$  s, respectively.).

**Table 2**  
Time cost of the regular wave cases.

Case	SPH		OceanWave3D		Coupling module		Total (h)
	Time (h)	Proportion	Time (h)	Proportion	Time (h)	Proportion	
1	9.39	0.83	0.21	0.02	1.71	0.15	11.31
2	9.55	0.80	0.72	0.06	1.74	0.15	12.01
3	9.36	0.84	0.08	0.01	1.68	0.15	11.12
4	9.24	0.80	0.57	0.05	1.76	0.15	11.57
5	9.44	0.84	0.09	0.01	1.68	0.15	11.21
6	2.00	0.65	0.21	0.07	0.89	0.29	3.11
7	41.17	0.87	0.21	0.01	6.14	0.13	47.52
8	9.41	0.83	0.2	0.02	1.21	0.11	10.82
9	9.69	0.83	0.21	0.02	2.32	0.20	12.22
10	0.00	0.00	0.62	1.0	0.00	0.00	0.62
11	23.18	1.00	0.00	0.00	0.00	0.00	23.18
Verbrugghe et al. [42] model	9.17	0.94	0.21	0.02	0.37	0.04	9.75

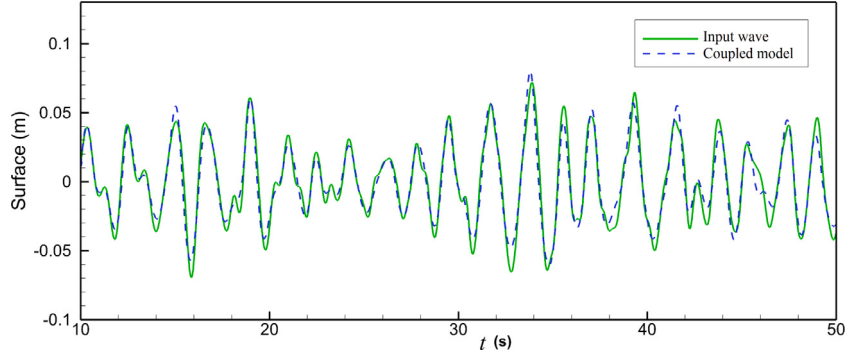


Fig. 13. Free surface comparison between coupled model and theory solution for irregular waves.

## 5.2. Irregular waves

To examine the performance of the coupled model in modelling irregular waves, a JONSWAP spectrum is selected to generate irregular waves with significant wave height  $H_s = 0.15$  m, peak period  $T_p = 2.0$  s for a water depth  $d = 0.66$  m. Initial particle spacing is 0.01 m, and the time step is 0.0001 s. The numerical domain for the coupled model is shown in Fig. 5. The coupling interface is at  $L_a = 6.0$  m. Mesh numbers is  $900 \times 10$  ( $x \times y$ ).

The water surface elevation measured at 15.0 m is plotted in Fig. 13. The theoretical time series is also represented for comparison. At local peaks, SPH results differ from theoretical values. There are two possible reasons for this: insufficient particle resolution and choice of relaxation domain length. Roselli et al. [70] and Altomare et al. [12] suggested that wave height should be more than ten times of particle resolution to achieve accurate modelling of regular waves. For the modelling of irregular waves, this condition may not be satisfied all over the free surface, affecting the accuracy of small wave heights in the irregular wave spectrum. The length of the relaxation domain may not be appropriate for all waves, either. Fig. 14 presents the contour of the velocity field at two representative moments. The velocity fields of the two numerical models are matched together at the coupling interface. The black lines indicate the free surface level in OceanWave3D. It can be found that the free surface evolution of OceanWave3D in the relaxation region is in good agreement with the SPH results.

## 5.3. Waves over a submerged bar

Regular wave propagation over a submerged bar [72] was simulated. The numerical flume, the geometric setup of the bar, and the position of four wave gauges (WG1–WG4) are shown in Fig. 15. Two regular waves of the same period  $T_w = 2.5$  s are simulated with different wave heights  $H_w$  of 0.022 m and 0.042 m. Non-breaking and spilling are observed, respectively, for the two examined wave

conditions. Different from the coupled SPH model for the empty wave tank as reported in Sections 5.1 and 5.2, three regions (except for the coupling regions) are applied for the present case: one SPH region in the middle of the wave tank covering the submerged bar, and two OceanWave3D regions occupying the remainder of the tank. The SPH region is from 6 m to 23 m. Regions simulated by OceanWave3D are from 0 m to 9 m and from 20 m to 40 m. Coupling regions are from 6.65 m to 9 m, and from 20 m to 22.35 m. Initial SPH particle spacing is 0.005 m. The numerical setup is shown in Table 3. The mesh spacing in OceanWave3D is much larger than the initial particle spacing in SPH. This is because the program crashes when it tries to use a denser particle spacing for case 3. A warning occurs when simulating wave breaking at higher resolutions.

Fig. 16 compares the free surface elevation at the four wave gauges (WG1–WG4). As the wave passes over the dam, the wave profile can be seen to be deformed. Comparing the coupled model, OceanWave3D and experimental results, it shows that the coupled model produces more accurate results at the local wave crests than the OceanWave3D. The high computational speed makes OceanWave3D attractive, although there is a slight decrease in computational accuracy. It is also important to note that the coupled model uses a much denser initial particle spacing than the grid employed in OceanWave3D.

Fig. 17 illustrates the evolution of the free surface for the regular wave with a higher wave height of 0.042 m. Fig. 18 illustrates the pressure field as well as the pressure field of the interface attachment. It shows that the interface pressure field remains smooth and stable at different moments in time. In Fig. 17(c) and (d), it can be observed that there is a large discrepancy between the OceanWave3D results and the experimental results, while the coupled model shows better agreement. Wave breaking occurs between  $x = 15.0$  m and 17.0 m. Fig. 19 shows the snapshots at different times of the coupled model and the OceanWave3D model at the bar. It can be seen that OceanWave3D's calculation nodes do not change in the horizontal direction, but move

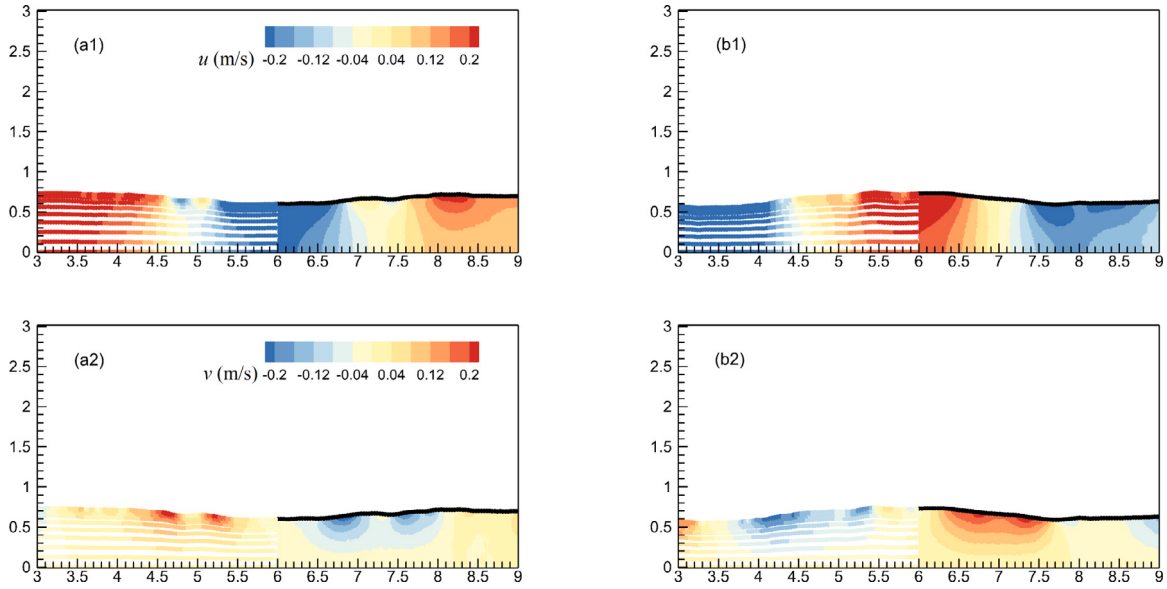


**Fig. 14.** Velocity field of irregular waves near coupling region at  $t = 28.2$  s and  $29.2$  s. (Labels 'a' and 'b' denotes  $28.2$  s and  $29.2$  s, respectively; Label '1' and '2' denotes horizontal velocity and vertical velocity, respectively. Black dots denote free surface level from OceanWave3D.).

**Table 3**  
Summary of the numerical setup of waves over a submerged bar.

Case	Mesh numbers ( $x, y$ )	Particle size (m)	Time step (s)	$H_w$ (m)	$T_w$ (s)	Breaking type	Cores	Cost (min)
s1	$500 \times 10$	–	0.01	0.022	2.5	Non-breaking	1	1
s2	$225 \times 10, 500 \times 10$	0.005	0.00001	0.022	2.5	Non-breaking	33	1217
s3	$500 \times 10$	–	0.01	0.042	2.5	Spilling	1	1
s4	$225 \times 10, 500 \times 10$	0.005	0.00001	0.042	2.5	Spilling	33	1217

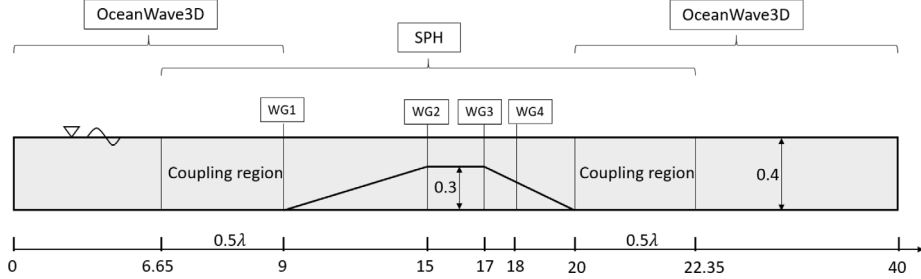


**Fig. 15.** Numerical setup for waves over a submerged bar.

in the vertical direction to simulate a wave passing over the bar. OceanWave3D is therefore not appropriate for simulating wave breaking. When the incident wave height is  $0.022$  m, OceanWave3D and SPH show similar wave propagation processes over the submerged bar. Overall, in the absence of non-breaking conditions, OceanWave3D's high efficiency makes it very competitive. In the case of wave breaking, OceanWave3D's results deviate far from the experimental results and the coupled model is the better choice. Also, as the SPH domain is reduced in the coupled model, the coupled model can further improve the efficiency compared to the SPH model.

#### 5.4. Oscillating water column

Finally, the coupled models are applied to simulate an onshore U-shaped Oscillating Water Column (U-OWC) device, which is a typical kind of wave energy converter [68,73]. The physical model tests were carried out in the wave-current flume at the University of Plymouth. The wave-current flume is 35 m long with a working section of 0.6 m wide and a maximum still water depth of 0.8 m. The U-OWC as shown in Fig. 20, was placed before the end of the flume with the back wall of

the structure at a distance of 27.0 m from the wave paddle. An orifice is used to simulate the damping of the turbine. The opening radius corresponds to an opening ratio of 0.7%. The corresponding damping factor is 1.47 according to the experimental data. Two pressure transducers (P1, P2) were placed at the top cover to measure the air pressure inside the chamber. Ru 1 and 2 are two wave gauges to record the surface level inside the chamber. The tests carried out in the numerical wave flume followed the set-up chosen in the laboratory tests. The entire numerical wave flume as shown in Fig. 21, is divided into two parts: the SPH region and the OceanWave3D region. Due to the considerable complexity and non-linear effects involved in the hydrodynamics of the OWC, the SPH model was used to simulate in the vicinity of the OWC. Wave generation and propagation are simulated using OceanWave3D until 18 m. After 18 m, the SPH model is used to capture non-linear phenomena. 18 m is the beginning of the coupling region and the length of the overlapping region is half wavelength 2.5 m. Fig. 22(a) shows 49 sub-domain divisions using 49 cores. 1 core is used for the OceanWave3D solver, whereas 48 cores are used for the SPH solver. Initial SPH particle spacing is 0.008 m. A constant time step of 0.00001 s is used, and the whole computation takes about 12 h for a 30 s

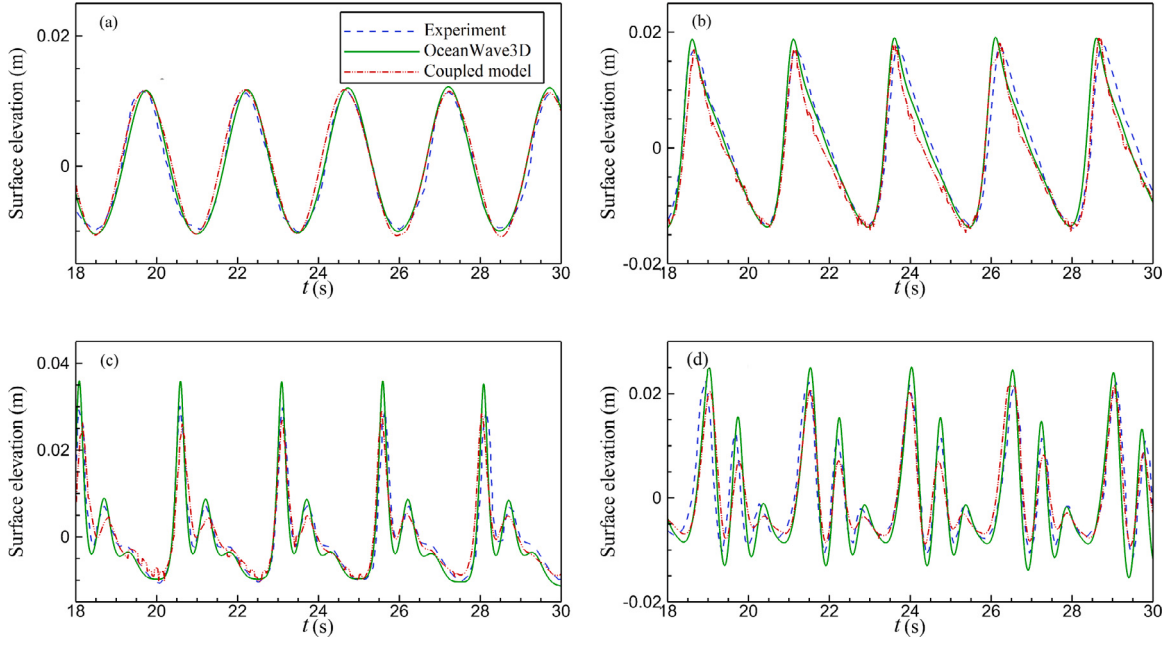


Fig. 16. Free surface elevations at the wave gauges WG1 (a), WG2 (b), WG3 (c), WG4 (d) for regular waves with wave period 2.5 s and wave height 0.022 m.

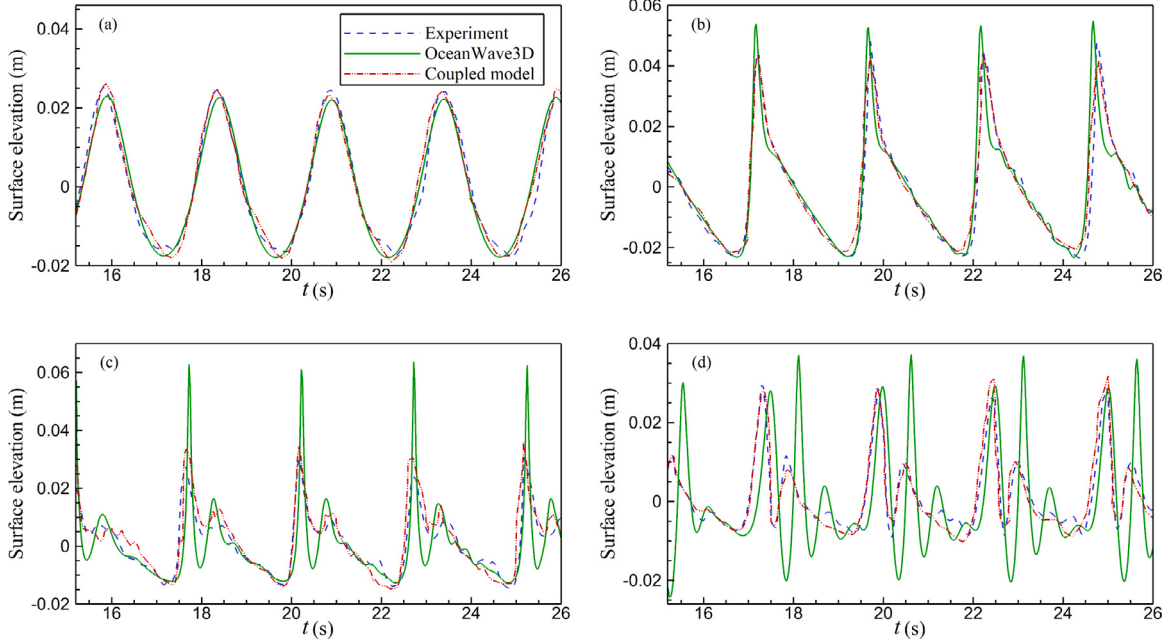


Fig. 17. Free surface elevations at the wave gauges WG1 (a), WG2 (b), WG3 (c), WG4 (d) for regular waves with wave period 2.5 s and wave height 0.042 m.

simulation. The single-phase SPH model with pneumatic model and regional ghost particle approach for the lip wall can be found in detail in [69,74].

Fig. 22 compares the surface elevation and air pressure drop inside the chamber of the coupled model with experimental data. The free surface elevation and air pressure predicted by the coupled model agree well with the experimental data, although a mild phase difference is observed before 19.5 s. Fig. 23 shows the pressure, horizontal and vertical velocity fields. Smooth numerical solutions can be found near the coupling interface. Also, the variation of the velocity field from 15 m to 18 m in the OceanWave3D region shows that the two-way coupled model can transfer reflected wave effects into OceanWave3D. In Fig. 24, complex free surface conditions qualitatively agree well with

the experiment at  $t = 21.4$  s and  $22.4$  s. At  $t = 21.4$  s, a rolling wave in the front of the submerged wall can be observed. The height of the free surface level inside the chamber is greater than the height of the free surface level in front of the lip wall at  $21.4$  s. At  $22.4$  s, the splash generated by the wave slamming against the lip wall can be reproduced. Fig. 24 demonstrates the good capability of the coupled model in modelling non-linear free surfaces.

The time history of mass and momentum of part of the SPH model of OWC example are shown in Fig. 25. The mass and momentum conservation of the system is not affected by the formation and deletion of free-surface particles before 10 s. After 10 s, the free surface particle generation/deletion leads to the change of mass and momentum of the system. The maximum differences in mass and momentum of

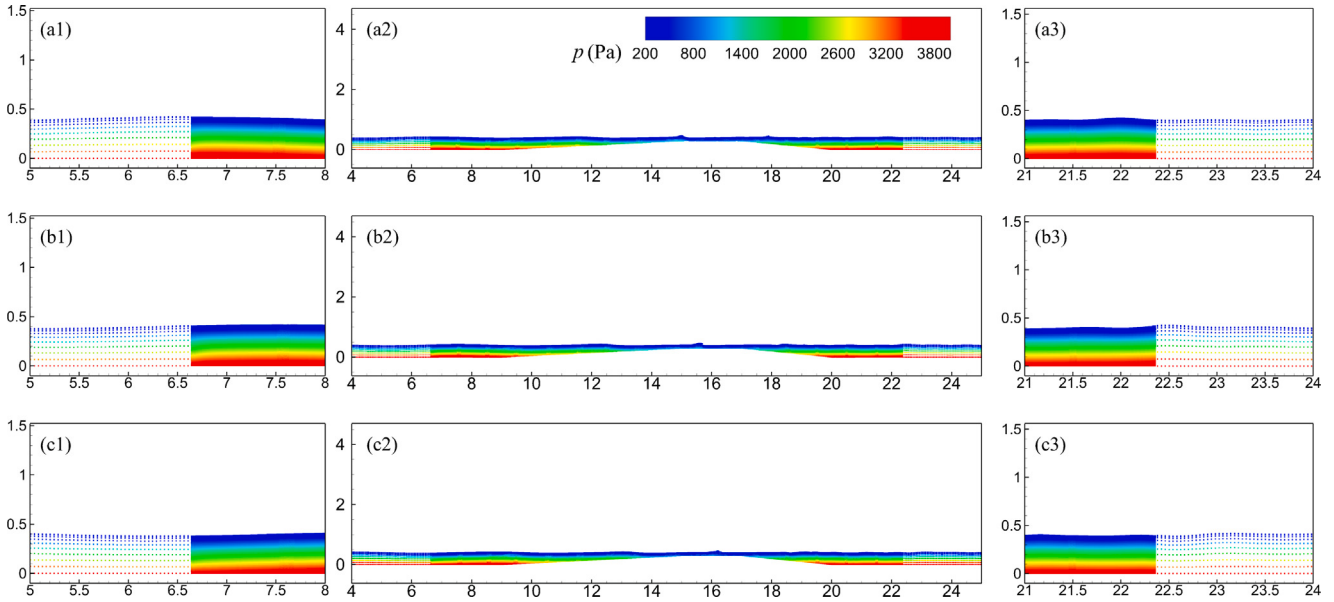


**Fig. 18.** Pressure field near the left coupling interface (1), near the bar region (2), and near the right coupling interface (3) at  $t = 18.5$  s (a),  $19.0$  s (b), and  $19.5$  s (c) predicted by the coupled model for wave period  $2.5$  s and wave height  $0.042$  m.

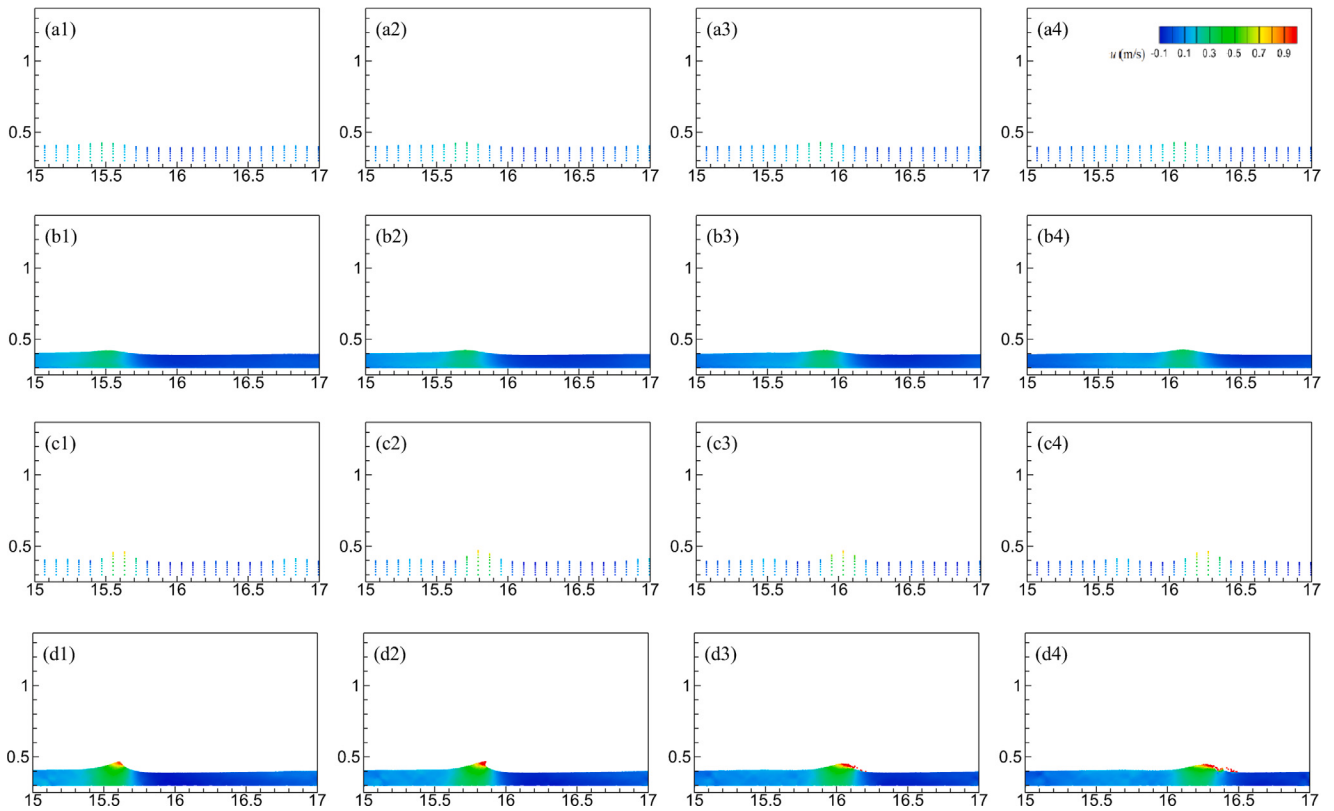


**Fig. 19.** Contour plot of the horizontal velocity above the submerged bar for wave period  $2.5$  s and wave height  $0.042$  m: OceanWave3D (a) and (c), coupled model (b) and (d) at  $t = 22.75$  s (1),  $23.05$  s (2),  $23.25$  s (3), and  $23.75$  s (4).

-0.69% and -3.88% both occur at 29.69 s. The difference in mass and momentum between with and without free surface particle generation can be calculated as

$$E_m = \frac{m_{all}^{with} - m_{all}^{without}}{m_{all}^{with}}, \quad (37)$$

$$E_M = \frac{M_{all}^{with} - M_{all}^{without}}{M_{all}^{with}}, \quad (38)$$

where labels ‘with’ and ‘without’ denote the coupled model with and without free surface particle generation/deletion. Fig. 26 compares the effects of free surface particle generation and deletion on the horizontal velocity distribution. At 29.5 s and 30.0 s, the results show an unsmoothed free surface and instability of the horizontal velocity field. Some fluid particles splash out of the free surface. This may be due to the reflected wave reaching the relaxation region affecting the free surface. This resulted in a mismatch between the SPH free surface

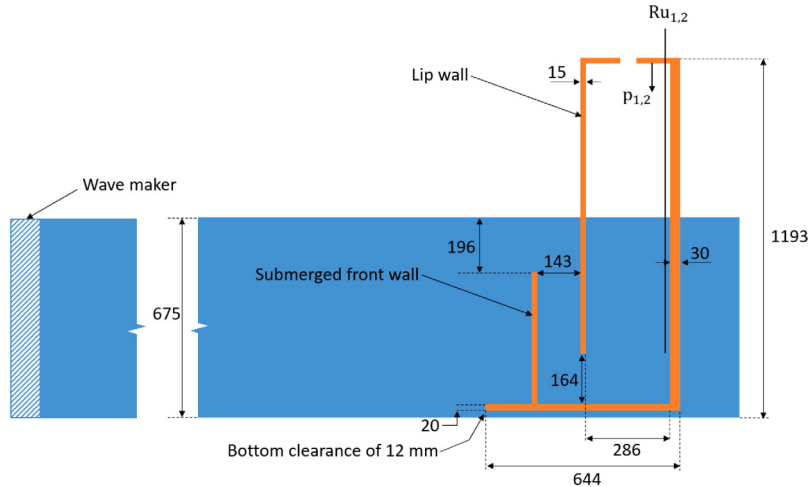


Fig. 20. Cross sectional of the U-OWC in the wave tank.

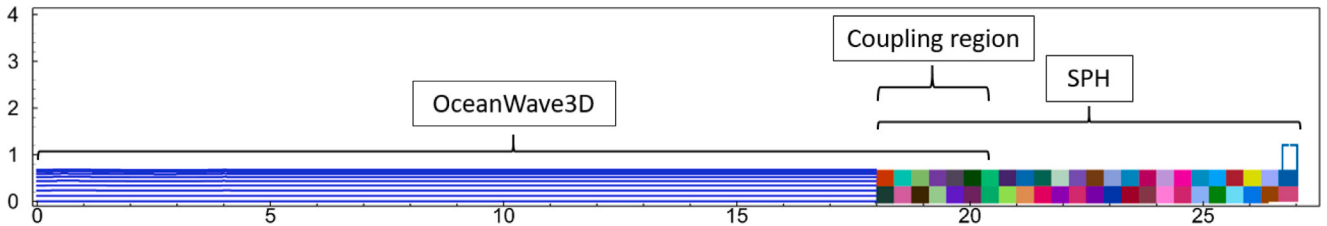


Fig. 21. Subdomain distribution of the coupling wave tank [73].

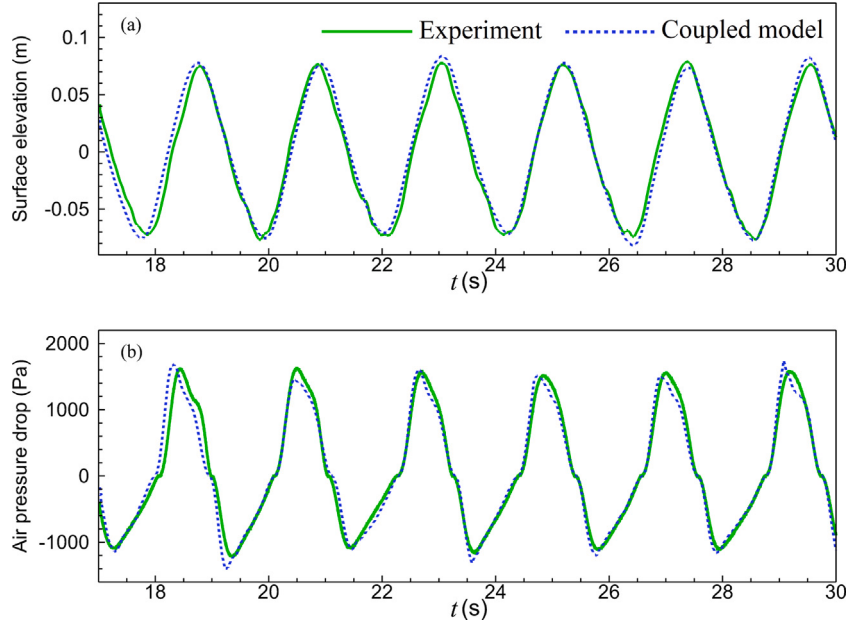


Fig. 22. Time series of surface elevation (a) and air pressure drop (b) inside the chamber.

and the OceanWave3D free surface in the coupling region. Although the technique may result in changes in mass and momentum, it can resolve free surface instability and ensure the stability of the calculation.

## 6. Conclusions

In this work, a two-dimensional two-way coupled model is proposed to hybridize the SPH model with OceanWave3D for the simulation

of nonlinear waves. The SPH model is used to simulate the nonlinear regions, while the remainder of the domain is simulated with OceanWave3D with high computation efficiency, which is based on a fully nonlinear potential flow theory. SPH and OceanWave3D are overlapping at the coupling region and take the same time step. In the SPH model, the open relaxation boundary is used in the coupling region. Horizontal velocity and free surface elevation in the open zone are obtained from OceanWave3D, while vertical velocity and density are obtained from the relaxation region by MLS reconstruction. The

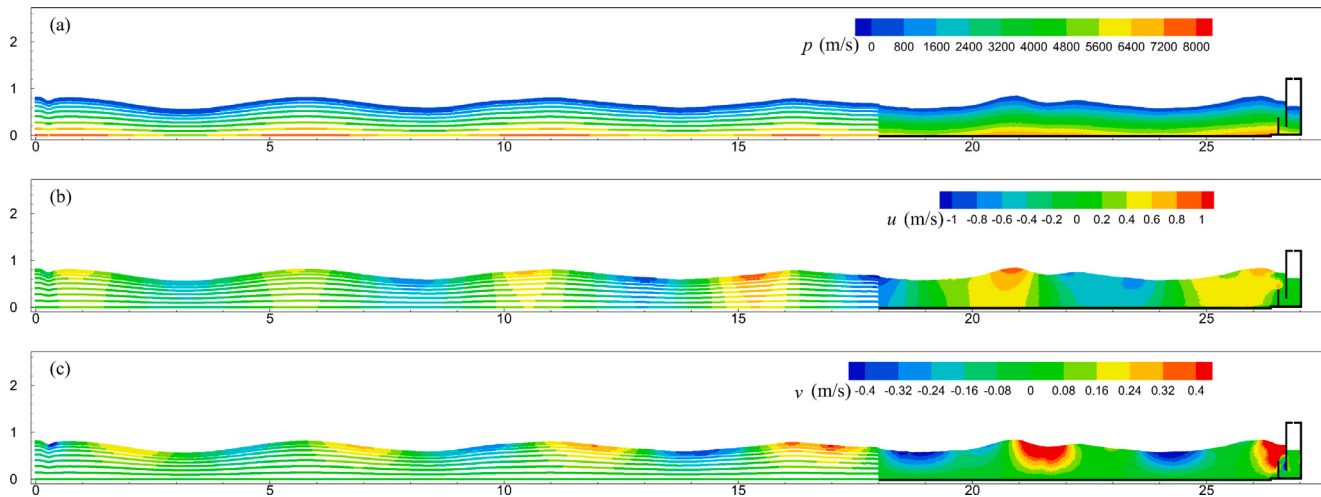


Fig. 23. Pressure (a), horizontal velocity (b) and vertical velocity (c) field at 22.0 s.

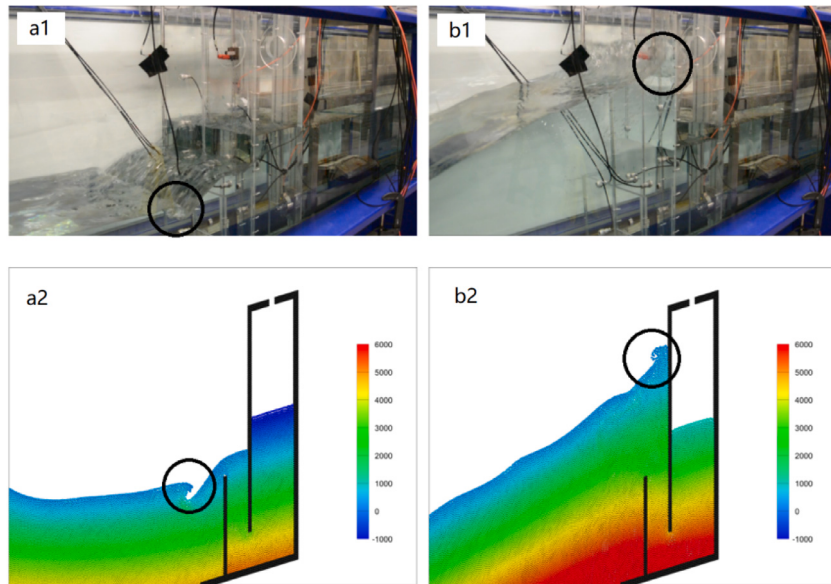


Fig. 24. Comparisons of non-linear free surface between the SPH and experiment at  $t = 21.4$  s and  $22.4$  s. (Labels 'a' and 'b' denotes 21.4 s and 22.4 s, respectively; Label '1' and '2' denotes experiment photos and numerical screenshots, respectively.).

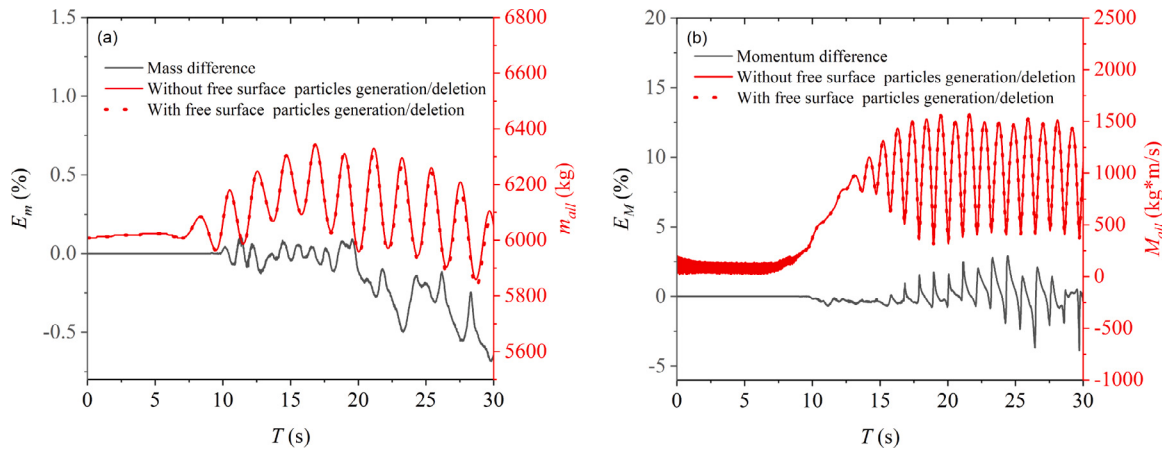
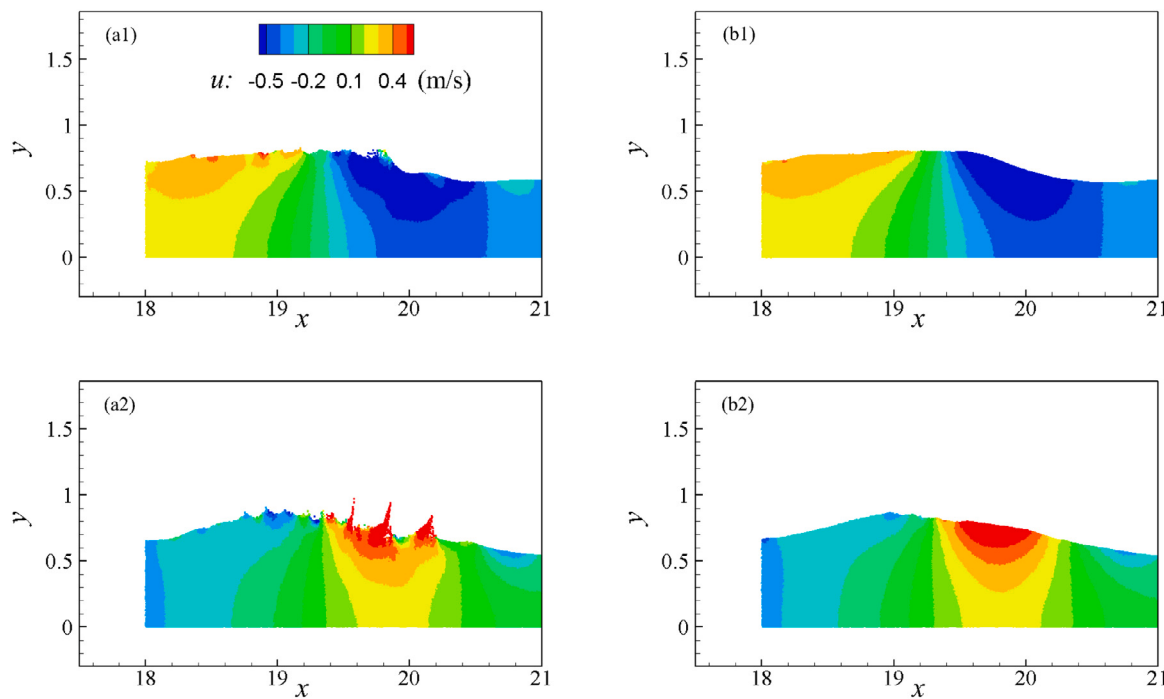


Fig. 25. Time history of the mass (a) and moment (b) of the OWC case with/without free surface particles generation/deletion. (Labels  $E_m$  and  $E_M$  denote the difference of mass and moment between the model with free surface particle generation/deletion and the model without free surface particles generation/deletion, respectively; Label  $m_{all}$  and  $M_{all}$  denote mass and moment of the SPH system, respectively.).



**Fig. 26.** Horizontal velocity field of OWC case with/without free surface particles generation/deletion near coupling region at  $t = 29.5$  s and  $30.0$  s. (Labels 'a' and 'b' denote with and without free surface particles generation/deletion, respectively; Labels '1' and '2' denote  $29.5$  s and  $30.0$  s, respectively.).

relaxation function is used in the relaxation region to couple the horizontal velocity and the free surface level from the OceanWave3D. The coupling of the free surface height in the relaxation region is achieved by the free surface particle generation/deletion. The free surface boundary conditions in the OceanWave3D coupling region are also coupled by the relaxation function. The coupled model is calculated in an OpenMPI parallel framework, where OceanWave3D is assigned only one processor to calculate it, while the MPI-based parallel SPH model is calculated using multiple processors in the SPH region.

The coupled model is tested for several cases including regular waves, irregular waves, waves over a submerged bar, and U-OWC device in regular waves. The results show that the coupled model can be highly accurate and efficient for wave hydrodynamics. The present coupled model can provide smoothed coupling interfaces. The development of coupled models has shortened the SPH computational domain. As a result, coupled models have lower computational costs than SPH-only models. At the same time, the coupled model retains the ability of the SPH model to deal with nonlinear surfaces.

However, this two-way coupling approach has some limitations. The current models are limited to simulating only two-dimensional problems. It will be necessary to expand to three-dimensional models in the future. The coupling region needs to be optimized. Specifically, the coupling coefficient, coupling position and coupling region length need to be studied to provide a reference for the coupling setting of specific problems.

#### CRediT authorship contribution statement

**Guixun Zhu:** Conceptualization, Methodology, Formal analysis, Validation, Writing – original draft, Writing – review & editing. **Jason Hughes:** Methodology, Writing – review & editing, Supervision. **Siming Zheng:** Conceptualization, Writing – review & editing, Supervision. **Deborah Greaves:** Conceptualization, Writing – review & editing, Supervision.

#### Declaration of competing interest

The authors declare that they have no known competing financial interests or personal relationships that could have appeared to influence the work reported in this paper.

#### Data availability

Data will be made available on request.

#### Acknowledgements

Guixun Zhu was supported by the financial support from China Scholarship Council (Grant No. 201806060137). The authors wish to thank Dr John Samuel for providing the experimental data of the U-OWC device used in this study. Deborah Greaves gratefully acknowledges the EPSRC, United Kingdom for supporting part of this work through the Supergen ORE Hub, EP/S000747/1.

#### References

- [1] Gingold RA, Monaghan JJ. Smoothed particle hydrodynamics: theory and application to non-spherical stars. *Mon Not R Astron Soc* 1977;181(3):375–89.
- [2] Lucy LB. A numerical approach to the testing of the fission hypothesis. *Astron J* 1977;82:1013–24.
- [3] Violeau D, Rogers BD. Smoothed particle hydrodynamics (SPH) for free-surface flows: Past, present and future. *J Hydraul Res* 2016;54(1):1–26.
- [4] Wang Z-B, Chen R, Wang H, Liao Q, Zhu X, Li S-Z. An overview of smoothed particle hydrodynamics for simulating multiphase flow. *Appl Math Model* 2016;40(23–24):9625–55.
- [5] Shadloo MS, Oger G, Le Touzé D. Smoothed particle hydrodynamics method for fluid flows, towards industrial applications: Motivations, current state, and challenges. *Comput & Fluids* 2016;136:11–34.
- [6] Ye T, Pan D, Huang C, Liu M. Smoothed particle hydrodynamics (SPH) for complex fluid flows: Recent developments in methodology and applications. *Phys Fluids* 2019;31(1):011301.
- [7] Vacondio R, Altomare C, De Leffe M, Hu X, Le Touzé D, Lind S, Marongiu J-C, Marrone S, Rogers BD, Souto-Iglesias A. Grand challenges for smoothed particle hydrodynamics numerical schemes. *Comput Part Mech* 2021;8(3):575–88.
- [8] Luo M, Khayyer A, Lin P. Particle methods in ocean and coastal engineering. *Appl Ocean Res* 2021;114:102734.

- [9] Goto H, Khayyer A, Shimizu Y. Entirely Lagrangian meshfree computational methods for hydroelastic fluid-structure interactions in ocean engineering—Reliability, adaptivity and generality. *Appl Ocean Res* 2021;115:102822.
- [10] Lyu H-G, Sun P-N, Huang X-T, Zhong S-Y, Peng Y-X, Jiang T, Ji C-N. A review of SPH techniques for hydrodynamic simulations of ocean energy devices. *Energies* 2022;15(2):502.
- [11] Lo EY, Shao S. Simulation of near-shore solitary wave mechanics by an incompressible SPH method. *Appl Ocean Res* 2002;24(5):275–86.
- [12] Altomare C, Dominguez JM, Crespo AJC, González-Cao J, Suzuki T, Gómez-Gesteira M, Troch P. Long-crested wave generation and absorption for SPH-based DualSPHysics model. *Coast Eng* 2017;127:37–54.
- [13] Shao S, Ji C, Graham DI, Reeve DE, James PW, Chadwick AJ. Simulation of wave overtopping by an incompressible SPH model. *Coast Eng* 2006;53(9):723–35.
- [14] Marrone S, Bouscasse B, Colagrossi A, Antuono M. Study of ship wave breaking patterns using 3D parallel SPH simulations. *Comput & Fluids* 2012;69:54–66.
- [15] He F, Zhang H, Huang C, Liu M. Numerical investigation of the solitary wave breaking over a slope by using the finite particle method. *Coast Eng* 2020;156:103617.
- [16] Zhang F, Crespo A, Altomare C, Domínguez J, Marzocca A, Shang S-p, Gómez-Gesteira M. DualSPHysics: a numerical tool to simulate real breakwaters. *J Hydronaut* 2018;30:95–105.
- [17] Liu M, Zhang Z. Smoothed particle hydrodynamics (SPH) for modeling fluid-structure interactions. *Science China Physics, Mechanics and Astronomy* 2019;62:984701.
- [18] Altomare C, Tafuni A, Domínguez JM, Crespo AJ, Gironella X, Sospedra J. SPH simulations of real sea waves impacting a large-scale structure. *J Mar Sci Eng* 2020;8(10):826.
- [19] Yamamoto T, Yasuda T, Oguma K, Matsushita H. Numerical simulation of scattering process of armour blocks on additional rubble mound behind breakwater during tsunami overflow using SPH method. *Comput Part Mech* 2021;1–16.
- [20] Mitsui J, Altomare C, Crespo AJ, Domínguez JM, Martínez-Estevez I, Suzuki T, Kubota S-i, Gómez-Gesteira M. DualSPHysics modelling to analyse the response of Tetrapods against solitary wave. *Coast Eng* 2023;183:104315.
- [21] Crespo AJ, Domínguez JM, Rogers BD, Gómez-Gesteira M, Longshaw S, Canelas R, Vacondio R, Barreiro A, García-Feal O. DualSPHysics: Open-source parallel CFD solver based on smoothed particle hydrodynamics (SPH). *Comput Phys Comm* 2015;187:204–16.
- [22] Guo X, Rogers BD, Lind S, Stansby PK. New massively parallel scheme for incompressible smoothed particle hydrodynamics (ISPH) for highly nonlinear and distorted flow. *Comput Phys Comm* 2018;233:16–28.
- [23] Oger G, Le Touzé D, Guibert D, De Leffe M, Biddiscombe J, Soumagne J, Piccinini J-G. On distributed memory MPI-based parallelization of SPH codes in massive HPC context. *Comput Phys Comm* 2016;200:1–14.
- [24] Chow AD, Rogers BD, Lind SJ, Stansby PK. Numerical wave basin using incompressible smoothed particle hydrodynamics (ISPH) on a single GPU with vertical cylinder test cases. *Comput & Fluids* 2019;179:543–62.
- [25] Ji Z, Fu L, Hu XY, Adams NA. A new multi-resolution parallel framework for SPH. *Comput Methods Appl Mech Engn* 2019;346:1156–78.
- [26] Zhang C, Rezavand M, Zhu Y, Yu Y, Wu D, Zhang W, Wang J, Hu X. SPHinXsys: an open-source multi-physics and multi-resolution library based on smoothed particle hydrodynamics. *Comput Phys Comm* 2021;267:108066.
- [27] Vacondio R, Rogers B, Stansby PK, Mignosa P, Feldman J. Variable resolution for SPH: A dynamic particle coalescing and splitting scheme. *Comput Methods Appl Mech Engrg* 2013;256:132–48.
- [28] Hu W, Pan W, Rakhsa M, Tian Q, Hu H, Negruț D. A consistent multi-resolution smoothed particle hydrodynamics method. *Comput Methods Appl Mech Engrg* 2017;324:278–99.
- [29] Sun P, Colagrossi A, Marrone S, Zhang A. The  $\delta$ -plus-SPH model: Simple procedures for a further improvement of the SPH scheme. *Comput Methods Appl Mech Engrg* 2017;315:25–49.
- [30] Yang X, Kong S-C, Liu M, Liu Q. Smoothed particle hydrodynamics with adaptive spatial resolution (SPH-ASR) for free surface flows. *J Comput Phys* 2021;443:110539.
- [31] Zhang Z, Liu M. A decoupled finite particle method for modeling incompressible flows with free surfaces. *Appl Math Model* 2018;60:606–33.
- [32] Zhang C, Rezavand M, Hu X. Dual-criteria time stepping for weakly compressible smoothed particle hydrodynamics. *J Comput Phys* 2020;404:109135.
- [33] Achim CV, Rozas RE, Toledo PG. Semi-decoupled first-order correction for smoothed particle hydrodynamics. *Appl Math Model* 2021;93:314–25.
- [34] Narayanaswamy M, Crespo AJC, Gómez-Gesteira M, Dalrymple RA. SPHysics-FUNWAVE hybrid model for coastal wave propagation. *J Hydraul Res* 2010;48(sup1):85–93.
- [35] Kirby J, Wei G, Chen Q, Kennedy AB, Dalrymple RA. Fully nonlinear Boussinesq wave model documentation and user's manual. Research Rep. CACR-98-06, Center for Applied Coastal Research, University of Delaware, Newark; 1998.
- [36] Altomare C, Crespo AJ, Rogers B, Dominguez J, Gironella X, Gómez-Gesteira M. Numerical modelling of armour block sea breakwater with smoothed particle hydrodynamics. *Comput Struct* 2014;130:34–45.
- [37] Altomare C, Tagliafierro B, Dominguez J, Suzuki T, Viccione G. Improved relaxation zone method in SPH-based model for coastal engineering applications. *Appl Ocean Res* 2018;81:15–33.
- [38] Napoli E, De Marchis M, Gianguzzi C, Milici B, Monteleone A. A coupled finite volume–smoothed particle hydrodynamics method for incompressible flows. *Comput Methods Appl Mech Engrg* 2016;310:674–93.
- [39] Marrone S, Di Mascio A, Le Touzé D. Coupling of smoothed particle hydrodynamics with finite volume method for free-surface flows. *J Comput Phys* 2016;310:161–80.
- [40] Chiron L, Marrone S, Di Mascio A, Le Touzé D. Coupled SPH–FV method with net vorticity and mass transfer. *J Comput Phys* 2018;364:111–36.
- [41] Zhang N, Yan S, Zheng X, Ma Q. A 3D hybrid model coupling SPH and QALE-FEM for simulating nonlinear wave-structure interaction. *Int J Offshore Polar Eng* 2020;30(01):11–9.
- [42] Verbrugge T, Stratigaki V, Altomare C, Domínguez J, Troch P, Kortenhaus A. Implementation of open boundaries within a two-way coupled SPH model to simulate nonlinear wave-structure interactions. *Energies* 2019;12(4):697.
- [43] Ni X, Feng W, Huang S, Zhao X, Li X. Hybrid SW-NS SPH models using open boundary conditions for simulation of free-surface flows. *Ocean Eng* 2020;196:106845.
- [44] Ni X, Feng W, Huang S, Zhang Y, Feng X. A SPH numerical wave flume with non-reflective open boundary conditions. *Ocean Eng* 2018;163:483–501.
- [45] Dalrymple RA, Rogers B. Numerical modeling of water waves with the SPH method. *Coast Eng* 2006;53(2–3):141–7.
- [46] Crespo A, Gómez-Gesteira M, Narayanaswamy M, Dalrymple R. A hybrid Boussinesq-SPH model for coastal wave propagation. In: Proceedings of the 3rd SPHERIC workshop, ERCOFATC.. Lausanne, Switzerland; 2008.
- [47] Fourtakas G, Stansby PK, Rogers BD, Lind SJ, Yan S, Ma Q. On the coupling of incompressible SPH with a finite element potential flow solver for nonlinear free-surface flows. *Int J Offshore Polar Eng* 2018;28(03):248–54.
- [48] Verbrugge T, Domínguez JM, Crespo AJ, Altomare C, Stratigaki V, Troch P, Kortenhaus A. Coupling methodology for smoothed particle hydrodynamics modelling of non-linear wave-structure interactions. *Coast Eng* 2018;138:184–98.
- [49] Zhang Z, Long T, Chang J, Liu M. A smoothed particle element method (SPEM) for modeling fluid-structure interaction problems with large fluid deformations. *Comput Methods Appl Mech Engrg* 2019;356:261–93.
- [50] Lin C, Wang X, Pastor M, Zhang T, Li T, Lin C, Su Y, Li Y, Weng K. Application of a hybrid SPH-Boussinesq model to predict the lifecycle of landslide-generated waves. *Ocean Eng* 2021;223:108658.
- [51] Ferrand M, Joly A, Kassiotis C, Violeau D, Leroy A, Morel F-X, Rogers BD. Unsteady open boundaries for SPH using semi-analytical conditions and Riemann solver in 2D. *Comput Phys Comm* 2017;210:29–44.
- [52] Antuono M, Colagrossi A, Marrone S, Lugni C. Propagation of gravity waves through an SPH scheme with numerical diffusive terms. *Comput Phys Comm* 2011;182(4):866–77.
- [53] Marrone S, Antuono M, Colagrossi A, Colicchio G, Touzé DL, Graziani G.  $\delta$ -SPH model for simulating violent impact flows. *Comput Methods Appl Mech Engrg* 2011;200(13):1526–42.
- [54] Colagrossi A, Landrini M. Numerical simulation of interfacial flows by smoothed particle hydrodynamics. *J Comput Phys* 2003;191(2):448–75.
- [55] Monaghan JJ. On the problem of penetration in particle methods. *J Comput Phys* 1989;82(1):1–15.
- [56] Bouscasse B, Colagrossi A, Marrone S, Antuono M. Nonlinear water wave interaction with floating bodies in SPH. *J Fluids Struct* 2013;42:112–29.
- [57] Engsig-Karup AP, Bingham HB, Lindberg O. An efficient flexible-order model for 3D nonlinear water waves. *J Comput Phys* 2009;228(6):2100–18.
- [58] Bingham HB, Zhang H. On the accuracy of finite-difference solutions for nonlinear water waves. *J Eng Math* 2007;58(1):211–28.
- [59] Currie IG. Fundamental mechanics of fluids. CRC Press; 2016.
- [60] Larsen J, Dancy H. Open boundaries in short wave simulations—a new approach. *Coast Eng* 1983;7(3):285–97.
- [61] Alvarado-Rodríguez CE, Klapp J, Sigalotti LDG, Domínguez JM, de la Cruz Sánchez E. Nonreflecting outlet boundary conditions for incompressible flows using SPH. *Comput & Fluids* 2017;159:177–88.
- [62] Monteleone A, Monteforte M, Napoli E. Inflow/outflow pressure boundary conditions for smoothed particle hydrodynamics simulations of incompressible flows. *Comput & Fluids* 2017;159:9–22.
- [63] Mayer S, Garapon A, Sørensen LS. A fractional step method for unsteady free-surface flow with applications to non-linear wave dynamics. *Internat J Numer Methods Fluids* 1998;28(2):293–315.
- [64] Jacobsen NG, Fuhrman DR, Fredsøe Jr. A wave generation toolbox for the open-source CFD library: OpenFoam®. *Internat J Numer Methods Fluids* 2012;70(9):1073–88.
- [65] Marrone S, Colagrossi A, Le Touzé D, Graziani G. Fast free-surface detection and level-set function definition in SPH solvers. *J Comput Phys* 2010;229(10):3652–63.
- [66] Paulsen BT, Bredmose H, Bingham HB. An efficient domain decomposition strategy for wave loads on surface piercing circular cylinders. *Coast Eng* 2014;86:57–76.
- [67] Zhu G, Hughes J, Zheng S, Greaves D. A novel MPI-based parallel smoothed particle hydrodynamics framework with dynamic load balancing for free surface flow. *Comput Phys Comm* 2023;284:108608.
- [68] Zhu G. Towards the development of smoothed particle hydrodynamics model for oscillating water column devices (Ph.D. thesis), University of Plymouth; 2023.

- [69] Zhu G, Graham D, Zheng S, Hughes J, Greaves D. Hydrodynamics of onshore oscillating water column devices: A numerical study using smoothed particle hydrodynamics. *Ocean Eng* 2020;218:108226.
- [70] Roselli RAR, Vernengo G, Altomare C, Brizzolara S, Bonfiglio L, Guercio R. Ensuring numerical stability of wave propagation by tuning model parameters using genetic algorithms and response surface methods. *Environ Model Softw* 2018;103:62–73.
- [71] Zago V, Schulze LJ, Bilotta G, Almashan N, Dalrymple R. Overcoming excessive numerical dissipation in SPH modeling of water waves. *Coast Eng* 2021;170:104018.
- [72] Beji S, Battjes J. Experimental investigation of wave propagation over a bar. *Coast Eng* 1993;19(1–2):151–62.
- [73] Zhu G, Samuel J, Zheng S, Hughes J, Simmonds D, Greaves D. Numerical investigation on the hydrodynamic performance of a 2D U-shaped oscillating water column wave energy converter. *Energy* 2023;274:127357.
- [74] Zhu G, Hughes J, Zheng S, Greaves D. A SPH model with open relaxation boundary for wave generation and absorption. In: The 31st international ocean and polar engineering conference. OnePetro; 2021.